

Measuring the Dielectric Constant of Liquid on a Chip with Silicon Nanowires

Scientific investigation of the measurement principles and functionality

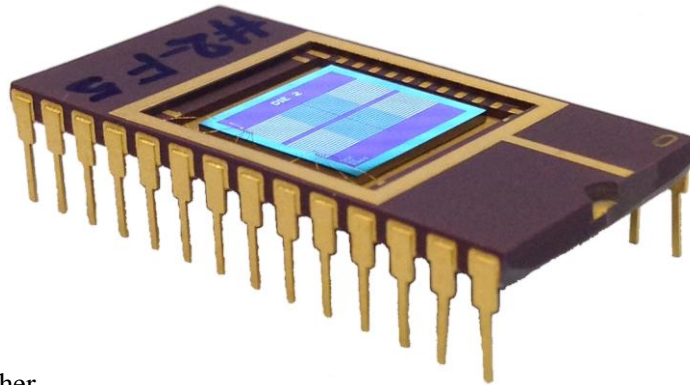
By Frank Bert Wiggers

A thesis submitted on April 7, 2013 in fulfillment of the requirements for the degree of

Master of Science in Electrical Engineering

at the

University of Twente



Supervisors

M.Sc. Marleen Mescher

Dr. ir. Johan H. Klootwijk

Prof. dr. ir. Rob A.M. Wolters

Graduation committee

Prof. dr. Jurriaan Schmitz

Prof. dr. ir. Rob A.M. Wolters

Dr. ir. Johan H. Klootwijk

Dr. Alexey Y. Kovalgin

Dr. Edwin T. Carlen

Details of author, supervisors and graduation committee members

Frank B. Wiggers

Master of Science student in Electrical Engineering, specialization: Microsystems and Microelectronics, at Semiconductor Components (SC) research group, University of Twente, *Enschede, The Netherlands*

M.Sc. Marleen Mescher - *Company supervisor*

Ph.D. student, Philips Research, *Eindhoven, The Netherlands*
marleen.mescher@philips.com

Dr. ir. Johan H. Klootwijk - *Committee member and Company supervisor*

Senior Scientist, Philips Research, *Eindhoven, The Netherlands*
johan.klootwijk@philips.com

Prof. dr. ir. Rob A.M. Wolters - *Committee member and University supervisor*

Professor at Semiconductor Components, University of Twente, *Enschede, The Netherlands*
Research fellow, NXP, *Eindhoven, The Netherlands*
r.a.m.wolters@utwente.nl

Prof. dr. Jurriaan Schmitz - *Committee member*

Chairs research group Semiconductor Components, University of Twente, *Enschede, The Netherlands*
j.schmitz@utwente.nl

Dr. Alexey Y. Kovalgin - *Committee member*

Assistant professor at Semiconductor Components, University of Twente, *Enschede, The Netherlands*
a.y.kovalgin@utwente.nl

Dr. Edwin T. Carlen - *Committee member*

Associate professor at Biomedical and Environmental Sensor Systems (BIOS), University of Twente, *Enschede, The Netherlands*
e.t.carlen@utwente.nl

The cover illustration shows a photograph of a die with silicon nanowires, in a chip package.

Title: Measuring the Dielectric Constant of Liquid on a Chip with Silicon Nanowires
Scientific investigation of the measurement principles and functionality

Author: F.B. Wiggers

Reviewers: M. Mescher, J.H. Klootwijk

Keywords: microfluidics, silicon nanowire, sensor, dielectric constant, water, dioxane, solvent, sealing, tubing, HMDS

Abstract: This project is about measuring the dielectric constant of liquid on a chip with silicon nanowires. This work is carried out under the umbrella of PhD research work on nanowire sensors, carried out by Marleen Mescher. This report comprises a theoretical description of nanowire sensors, which is combined with the device layout. In particular the liquid interfacing and the prevention of leakage when using solvents has been extensively studied. Dioxane has been selected as the liquid to complement water for characterization of the nanowire sensor, due to its low dielectric constant and miscibility. It was found that a sealing layer based on an acrylic adhesive on a polyester carrier proved sufficiently durable. In addition, silicone rubber has been identified as a suitable tubing material. These efforts resulted in a microfluidic setup that successfully contained the liquids for the duration of the experiments as reported in this research.

An important part of this work covers the comparison of experiments focusing on air, water, and 1,4-dioxane. A method to extract the threshold and slope parameters was defined and executed. Based on calculations and experimental evidence the nanowire sensor has been shown to work and a change in transconductance of the sensor was successfully measured between water and dioxane. Recommendations were made to improve the sensitivity and accuracy of these measurements. Important conclusions were also made relating to the measurement methodology. The first conclusion is that just one measurement is not reliable and stabilization is required. The second conclusion is that time and the number of measurements are important parameters in this stabilization process. And finally, for each specific system these parameters could behave differently, requiring the identification of the dominant parameter in order to develop a reliable measurement protocol.

Preface

In July 2012, I started my master thesis project at Philips Research in Eindhoven. There, I worked on the concept of measuring the dielectric constant of liquid on a chip with nanowire sensors. These nanowire sensors are the subject of Marleen's PhD research. I would like to thank her, because it was with Marleen's supervision and guidance that I was able to perform my research at such a unique place. I also want to thank Johan and Rob for their excellent guidance and for inspiring me with confidence and motivation when it was needed. For this opportunity and the advice and guidance you have all given me, I am truly grateful.

Frank Wiggers
March 18th, 2013

Table of Contents

Preface	v
Table of Contents	vii
1 Introduction	1
2 Operating Principle of Nanowire Sensors	2
2.1 Semiconductor Physics	2
2.2 Nanowire Sensor	2
2.3 Electrical Model	3
2.4 Sensing Mechanism	5
3 Nanowire Devices	7
3.1 Layout	7
3.2 Fabrication	7
4 Measurement Methodology	10
4.1 Setup	10
4.2 Settings.....	11
4.3 Measurement Artifacts	13
4.4 Parameter Extraction.....	16
4.5 Conclusion	18
5 Liquid Interfacing	19
5.1 Microfluidic Cap	20
5.2 Liquids	20
5.3 Tubing	23
5.4 Connectors	24
5.5 Sealing	25
5.6 Pump and Syringes.....	27
5.7 Conclusion	27
6 Experimental	28
6.1 Properties in Air	28
6.2 Properties in Water.....	32
6.3 Surface Modification.....	34
7 Conclusion	44
8 Recommendations	47
8.1 Experiments	47
8.2 Measurement Setup.....	47
8.3 Device Design	48
References	49

1 Introduction

Silicon nanowires are used in current research for the detection of a broad range of chemical compounds and biomolecules [1–4]. These sensors exhibit enhanced sensitivity, compared with regular planar field-effect transistors (FETs), originating from their advantageous surface-to-volume ratio [5], [6]. The selectivity can be adjusted through modification of the nanowire surface and used in this way for a broad range of target species, including DNA [3], protons [7], antibodies [4], and metal ions [8], [9]. These sensors have even been used for sensing the flow velocity of a solution [10]. Besides applications in aqueous media, these sensors have also been used in gas environments [11], [12].

Silicon nanowires however hold the potential to integrate and perform a second type of measurement. This measurement depends on capacitive coupling through the liquid media between the nanowire and the substrate. The integration of this second measurement technique can complement the analysis of the sensor system by measuring changes in the dielectric constant of the surrounding environment.

The challenge is to integrate this innovative measurement technique in silicon nanowires, which can also be used to sense surface reactions through surface charge interaction [6], [13], [14]. The aim of this research is to investigate the measurement principles of measuring the dielectric constant of liquid on chip with silicon nanowires and experimentally prove the functionality.

The theory on semiconductor physics and silicon nanowires is described in chapter 2. Chapter 3 explains the device layout and fabrication. The measurement setup and parameter extraction is discussed in chapter 4. The details of the setup regarding the liquid interfacing are detailed in chapter 5. The experimental results of measurements of the dielectric constant are treated in chapter 6. The conclusions are summarized in chapter 7 and the recommendations are listed in chapter 8.

2 Operating Principle of Nanowire Sensors

The aim of this chapter is to create an understanding for, and describe, the working principle of a nanowire sensor. The first section briefly treats the physics of semiconductor material and introduces its properties. The second section explains a field-effect transistor and how it uses the properties of semiconducting material. And finally, in the third section, the concept of a nanowire is explained, in particular how this device exploits the working principle of a field-effect transistor to create a connection with the external environment that allows it to function as a sensor.

2.1 Semiconductor Physics

Solid materials can be divided into three groups when their electrical properties are considered, i.e. the metals, the semiconductors, and the insulators. Their electrical properties can be explained using their respective energy band diagrams. These diagrams show the energy levels where states exist that can be occupied by electrons. Two energy bands are of particular importance: the valence and conduction band. The amount of energy separating these two bands is called the bandgap. Electrons will require energy to traverse this gap and one possible source for this is thermal energy.

In metals the valence and conduction band overlap. This allows many electrons to enter the conduction band with relatively little available thermal energy. Insulators cover the other extreme. Their valence and conduction band are separated by a very large bandgap.

Semiconductors include the materials whose bandgap is relatively small. At 0 K the valence band will be filled with electrons, leaving the conduction band completely empty. With an increase in thermal energy electrons will be able to enter the conduction band. However, because of the presence of a bandgap, the amount of mobile charge carriers is low even at room temperature. An important property however is that the conductivity can be altered significantly.

Silicon is the most well-known semiconductor and has a bandgap of 1.1 eV. This results in a theoretical electron density of 10^{11} cm^{-3} . This conductivity can be altered by doping the silicon. Doping involves substituting a small number of silicon atoms with atoms that either donate a free electron or accept an electron and create free holes. As a result the doping concentration will determine the charge carrier type and concentration. When electrons or holes are the majority carriers, the silicon is called n- or p-type, respectively.

2.2 Nanowire Sensor

Another way to alter the conductivity of a semiconductor can be accomplished by inducing a field-effect. This can for instance be realized by adding a dielectric layer with a conductor on top. In this way the semiconductor and conductor form the two electrodes of a capacitor. The conductor is referred to as the gate electrode. By applying a potential difference between these two electrodes, charge will accumulate on the electrodes according to:

$$Q = CV [C] \tag{1}$$

where Q is the charge on either electrode, C is the capacitance between the two electrodes, and V is the potential difference.

2.2.1 Operating Regions

According to the potential difference, the semiconductor can be operated in three regimes. In this case a p-type semiconductor is used, but the theory is analogue for n-type. And zero flatband voltage is assumed for sake of simplicity. A non-zero flatband voltage would imply an offset for the different regions. If the potential applied to the gate is negative with respect to the semiconductor, the semiconductor will operate in accumulation mode. Holes will be attracted to and accumulate near the

surface in the semiconductor and form a conductive sheet. If the potential applied to the gate is slightly positive with respect to the semiconductor, the semiconductor will operate in depletion mode. A negative charge will build up in the semiconductor, initially due to the depletion of the semiconductor starting from the oxide-semiconductor interface. The charge is due to the immobile and negatively charged dopant ions. The depletion layer width further increases with increasing gate voltage. As the potential becomes more positive another type of negative charge appears. Now electrons will start to accumulate near the surface instead. This operating region is called inversion.

Operating in the accumulation region, this increase in mobile charge carriers in the semiconductor results in an increase in conductivity. This can be detected by applying a small known potential across the semiconductor and measuring the current.

2.2.2 Surface-area-to-volume Ratio

The nanowire sensor is fabricated from p-type semiconductor and is shaped such to allow for a favorable surface-to-volume ratio. This means that surface effects can be distinguished better from the bulk. In this case the induced charge that accumulates near the surface increases the conductivity. For sensing purposes it is best to optimize for the ratio of greatest difference to average level in conductivity. For this reason one would like to eliminate the material that is not near the surface as it only adds bulk conductivity. One way to improve this ratio is by scaling down the sensor geometry:

$$\frac{\text{Surface area}}{\text{Volume}} = \frac{a^2}{a^3} = \frac{1}{a} \quad (2)$$

where a is the scaling factor of the geometry.

2.3 Electrical Model

The electrical behavior of the nanowire in accumulation-mode is modeled as shown in Fig. 1. The resistance R_{bottom} accounts for the resistance along the bottom side of the nanowire, where mobile charge carriers have accumulated. R_{top} accounts for the resistance along the sides and top of the nanowire structure, where mobile charge carriers have also accumulated. And finally, R_{bulk} accounts for the resistance of the silicon bulk of the nanowire. These three conduction paths contribute in parallel to the total resistance. To model the capacitive coupling between the gate and the nanowire the physical layout of the device is approximated by two capacitances as shown in Fig. 2. One represents the variable capacitance between the gate and the top and side surfaces of the nanowire, and is a function of the dielectric constant of the liquid. The other capacitance represents the constant capacitance between the gate electrode and bottom of the nanowire.

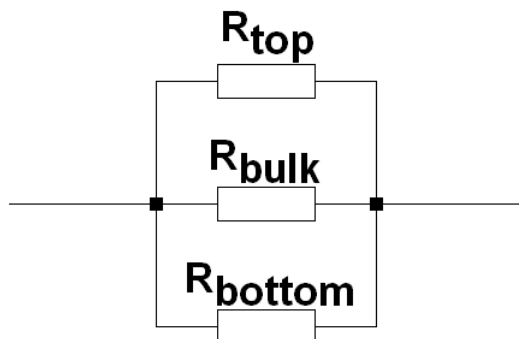


Fig. 1 Electrical model of the resistance of the silicon nanowire.

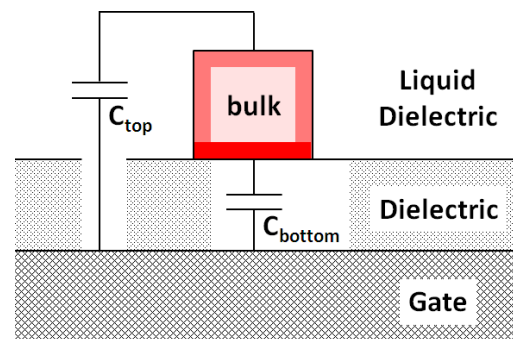


Fig. 2 Electrical model of the capacitive coupling to the silicon nanowire.

A first-order approximation of the current through a nanowire has been derived. As the resistances are in parallel, the separate currents can be summed accordingly:

$$I_{DS} = I_{bulk} + I_{bottom} + I_{top} \quad (3)$$

The bulk current is given by:

$$I_{bulk} = \mu_b q N_A \frac{WH}{L} V_{DS} \quad (4)$$

where μ_b is the bulk mobility of holes in silicon, q is the elementary charge, N_A is the acceptor doping concentration, W , H and L are respectively the width, height and length of the nanowire, and V_{DS} the potential difference applied across the nanowire. The current along the bottom is given by:

$$I_{bottom} = \mu_b \frac{W}{L} C_{bottom} |V_{GS} - V_{t,bottom}| V_{DS} \quad (5)$$

Where V_{GS} is the potential difference between the gate and the nanowire, $V_{t,bottom}$ is the accumulation threshold voltage of the bottom side, and C_{bottom} is the capacitance per area and is approximated as a parallel-plate capacitance:

$$C_{bottom} = \frac{\epsilon_r \epsilon_0}{t_{ox}} \quad (6)$$

where ϵ_r is the relative permittivity of silicon oxide, ϵ_0 is the vacuum permittivity, and t_{ox} is the silicon oxide layer thickness. The current along the side and top is given by:

$$I_{top} = \mu_b \frac{W + 2H}{L} C_{top} |V_{GS} - V_{t,top}| V_{DS} \quad (7)$$

Where $V_{t,top}$ is the accumulation threshold voltage of the top side of the nanowire, and C_{top} is the capacitance per area between the top side of the nanowire and the gate. Given the complex geometry of C_{top} (see Fig. 2) numerical simulation is required to estimate this.

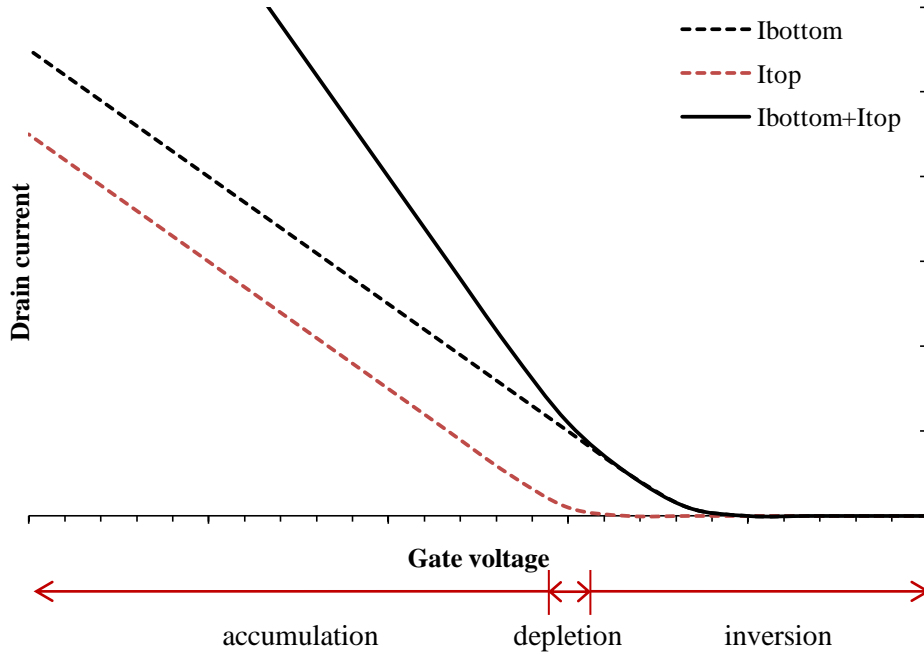


Fig. 3 Qualitative example of an I_D-V_G curve as based on theory. It shows the contribution from the top transistor (dashed red), bottom transistor (dashed black), and the sum (solid black). The operating regions for the top transistor are shown below the graph.

The total current is given by:

$$I_{DS} = V_{DS}\mu_b \left(qN_A \frac{WH}{L} + \frac{W}{L} C_{bottom} |V_{GS} - V_{t,bottom}| + \frac{W + 2H}{L} C_{top} |V_{GS} - V_{t,top}| \right) \quad (8)$$

From this it can be concluded that for a constant V_{DS} , the I_{DS} - V_{GS} curve will have a steeper slope due to the contribution of the top side accumulation and consequent conduction. The effect of surface charge is limited to shifting the accumulation region. Fig. 3 shows a qualitative theoretical example of an I_D - V_G curve and the different operating regions for the top transistor. The current contribution from the top transistor is chosen to be equal to that of the bottom transistor for illustrative purposes only. The contribution from the bulk current is not shown.

2.4 Sensing Mechanism

Opening up the sensor from the top allows for exposure to and thus influence of a variable environment. A semiconductor is particularly suitable for this purpose as its conductivity is sensitive to the associated changes in electric field.

2.4.1 Dielectric Constant

An important aspect of the nanowire sensor is that it is fabricated on top of silicon oxide, a dielectric. Because the sensor is exposed from the top and sides, a liquid can be introduced and its dielectric constant will influence the capacitive coupling between the gate electrode and the top and side surfaces of the nanowire. In this way a sensing mechanism is incorporated. The dielectric constant of the liquid on the nanowire influences the amount of charge that accumulates. This accumulated charge in turn can be sensed by measuring the conductivity of the nanowire.

This dielectric constant can be seen as a measure for the polarization of a material in response to an electric field [15]. The greater the polarization, the greater its dielectric constant. When an electric field is applied across a dielectric, the dielectric will polarize and generate an electric field opposite to it, cancelling it partially. However, when a constant voltage is applied the electric field is constant too. This means more charge will accumulate on the electrodes to establish the same electric field.

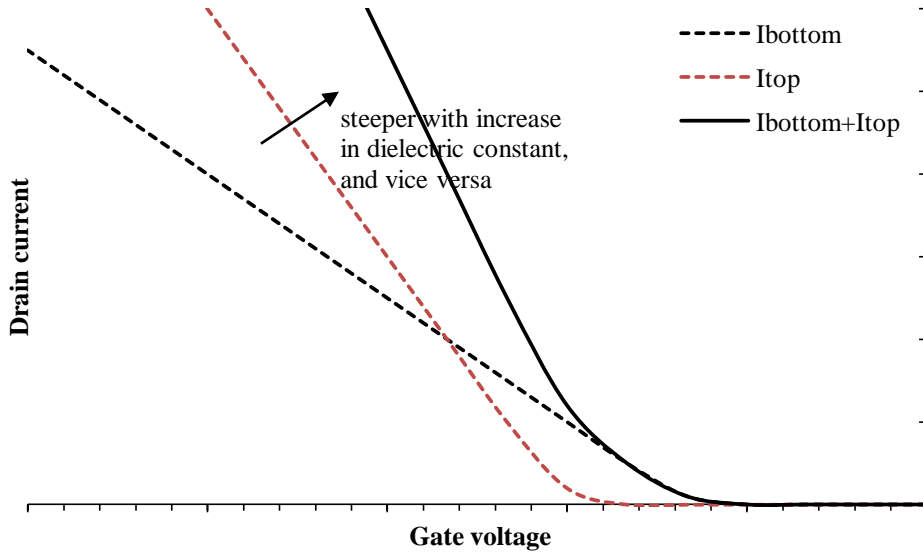


Fig. 4 Qualitative example of an I_D - V_G curve when the dielectric constant of the top environment is increased resulting in a larger top transistor current while the bottom transistor current remains constant. It shows the contribution from the top transistor (dashed red), bottom transistor (dashed black), and the sum (solid black).

It is therefore expected to measure higher currents in a nanowire that is surrounded by a liquid with a high dielectric constant compared to a liquid with a lower dielectric constant, for the same gate potential. This means that in an I_D - V_G curve it is expected to see a steeper slope for a higher dielectric constant. This is illustrated in Fig. 4.

2.4.2 Surface Charge

Charge on the surface of the gate oxide will attract the opposite type of charge in the semiconductor below. This is similar to the capacitance described before, where this surface charge can comparatively be related to an effective voltage across the oxide. Change in the surface charge can therefore be measured as a shift in the voltages for which the semiconductor changes operating regions.

The gate oxide comprises silicon oxide and its surface is covered with silanol groups. These groups deprotonate depending on the pH of the liquid in contact with the oxide surface, creating a negatively charged surface. In the case of p-type semiconductor operated in accumulation mode, an increase in positive surface charge will repel positively charged holes in the semiconductor. This effect can be measured and detected as a negative shift of the (gate) voltage for which accumulation-mode conduction starts to increase significantly. This is illustrated in Fig. 5.

Another advantage is that the sensitivity can be altered by modifying the surface with other molecules. These molecules can for example have a preferential binding to target molecules, or have a different acid dissociation constant.

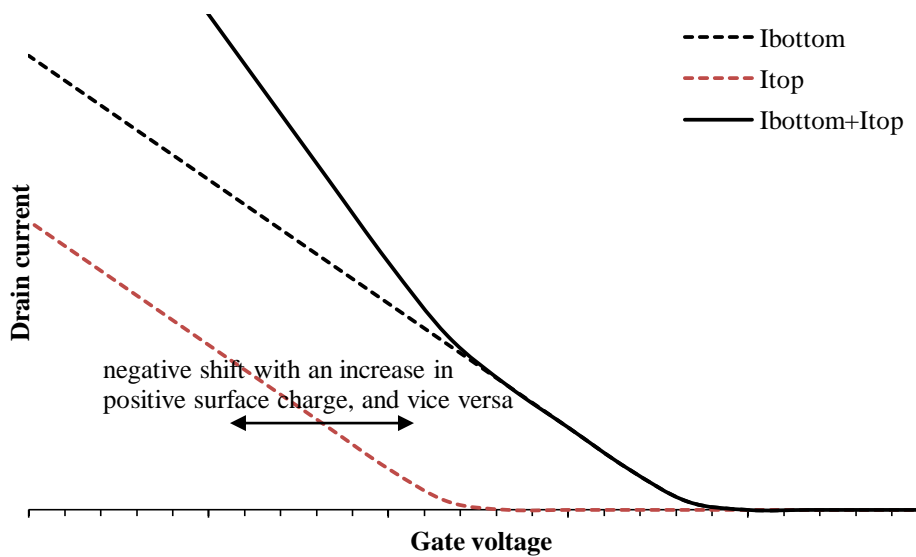


Fig. 5 Qualitative example of an I_D - V_G curve when the surface charge on the top surface changes, resulting in a shifted top transistor characteristic while the bottom transistor characteristic remains constant. It shows the contribution from the top transistor (dashed red), bottom transistor (dashed black), and the sum (solid black).

3 Nanowire Devices

The aim of this chapter is to describe the layout and fabrication of the nanowire sensors. The first section explains the layout of the sensors. The second section treats the processing steps used in order to fabricate these devices.

3.1 Layout

The layout of the chip with the silicon nanowire field effect transistors is shown in Fig. 6. Every die consists of two identical but mirrored columns of fourteen nanowire field-effect devices each. The sensing part of the device consists of a rectangular block of silicon, referred to as the nanowire. This nanowire is contacted on either end by highly-doped silicon contact leads. These leads are connected with a via to aluminum contacts on the surface of the chip. Wirebonds on these aluminum contacts help establish an electrical connection to the external characterization equipment. The important dimensions of the nanowire are determined by the structure that is etched from the silicon and by the no-implant wafer stepper reticle that is used to define the low-doped part of the actual nanowire. Die 1, 2 and 4 are identical and consist of nanowires with a width of 400 nm and a low-doped (effective device) length of 3 μm . Die 3 consists of nanowires with a low-doped length of 3 μm and a variation in widths (600, 1000, 1500 and 2000 nm). All nanowires have a height of 50-100 nm [16].

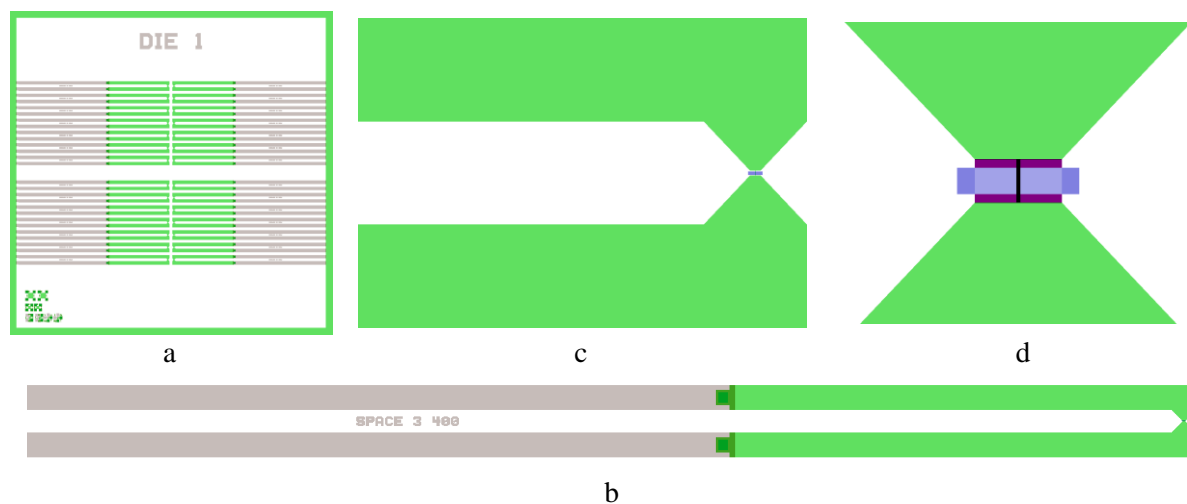


Fig. 6 Details of the wafer stepper reticles used. Grey parts are metal, green is silicon, blue is the no-implant area, dark purple is the opening in the silicon nitride passivation. a) Is the overview of a complete die, where on both sides two times fourteen devices are placed. The lower left corner contains test structures used for process control. b) Shows a single nanowire device: the metal contact leads are connected to the (highly doped) silicon connections, which connect to the nanowire. c) Shows how the leads come to the nanowire and d) shows the no-implant area (blue) and silicon nitride opening (dark purple) on top of the nanowire.

3.2 Fabrication

The devices are produced from 150 mm (6 inch) SOI wafers as described by [16]. The wafers have a buried oxide (BOX) layer of 300 nm and a high-doped (10^{19} cm^{-3}) substrate (Fig. 7a). The low-doped (10^{17} cm^{-3} p-type) device layer has a thickness of ~ 50 nm. Alignment markers are lasered in the wafer and etched free (Fig. 7b). Subsequently, a screen oxide is applied before the wafer is implanted to protect the wafer during the implantation. A layer of resist is applied and patterned, after which the wafer is implanted with boron (Fig. 7c-e). The resulting high doped, p-type areas will eventually be part of the contact pads and will form the source and drain terminals. Ultralow contact resistance ohmic contacts are thus formed. The low-doped area will become the actual nanowire, and thus the

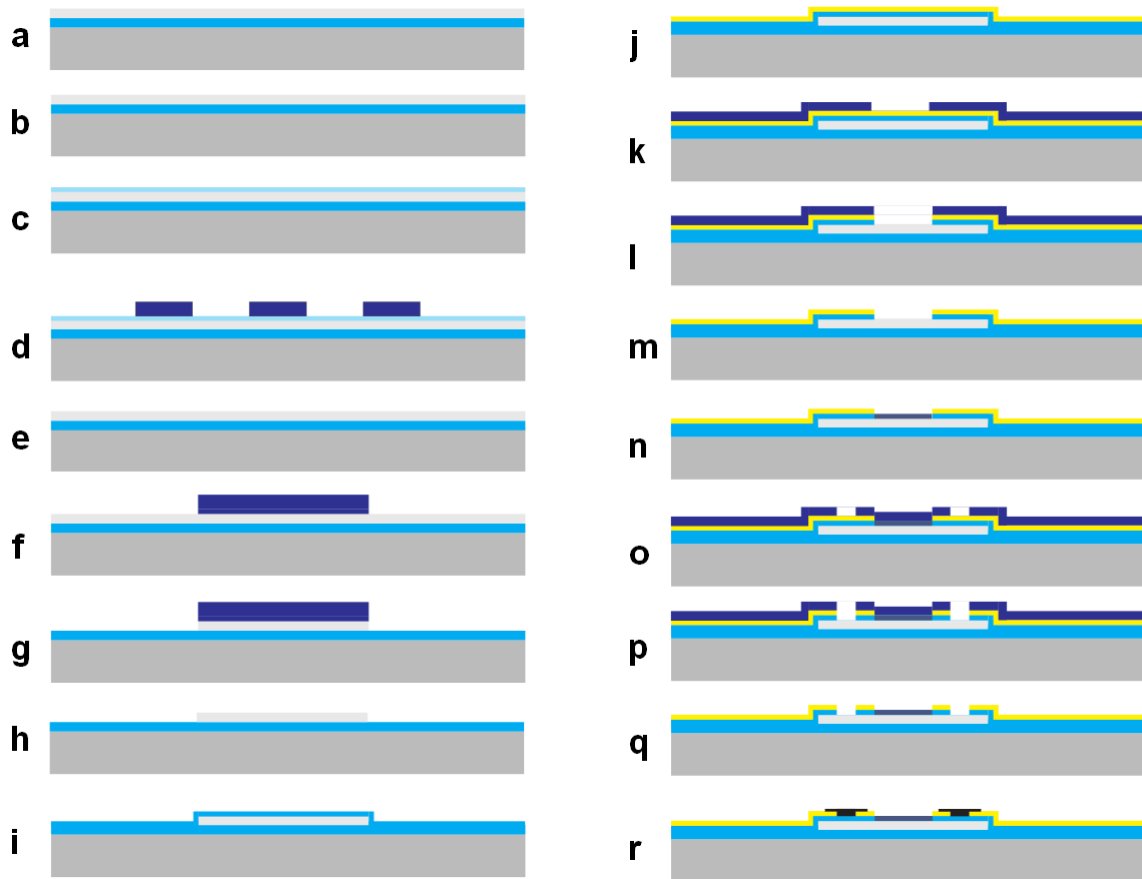


Fig. 7 Schematic representation of the process flow. Dark grey: high doped silicon, light grey: low doped silicon, light blue: silicon oxide (see text for type), dark blue: photoresist, black: metal, yellow: passivation layer a) SOI wafer b) with alignment markers c) SOI wafer with screen oxide d) no-implant mask on SOI wafer e) removal of screen oxide and no-implant mask after implantation f) mask for silicon etch g) silicon etching h) remaining silicon after etching i) growth of 20 nm oxide followed by deposition of 80 nm TEOS j) deposition of passivation layer k) mask for opening silicon oxide/passivation layer around nanowire surface l) etching to nanowire surface m) removal of etching mask n) front oxide growth o) contact hole lithography p) contact hole etching q) removal of mask r) metal deposition and patterning.

active and most important part of the device. The resist and the screen oxide are then removed from the implanted wafer, after which a new layer of resist is patterned to form a mask during the subsequent silicon etch (Fig. 7f-h). This step defines the dimensions of the nanowire and can be done by patterning using e-beam instead of a wafer stepper reticle to obtain even smaller nanowire dimensions. The resist is removed and 20 nm thermal oxide is grown on top of the silicon. This is then covered with 80 nm TEOS (Fig. 7i). The thermal oxide is used to ensure a good silicon-silicon dioxide interface, while the TEOS is used to thicken the silicon oxide layer. A passivation layer (silicon nitride in this specific example) of 100 nm is deposited afterwards (Fig. 7j). The oxide and the passivation layer will form an insulating layer to prevent breakdown when over etching of the silicon takes place. Furthermore, they will reduce the leakage current over the nanowire surface and protect the wafer against mechanical damage. However, the most important reason to use the passivation top layer is the possibility it provides for further modification; the nanowire will be covered with an oxide layer, while the rest of the die has e.g. a parylene top layer, enabling selective modification. It is noted that other passivation layers are also possible, as long as they either have a different surface termination than the front oxide, or are resistant to the etching with (diluted) HF, which is typically used in the formation of hydrogen-terminated silicon. This combination of protecting layers is covered with resist, which is patterned such that only the silicon nanowire is left exposed (Fig. 7k-m). This step is followed by the growth of a front oxide layer on top of the nanowire (Fig. 7n).

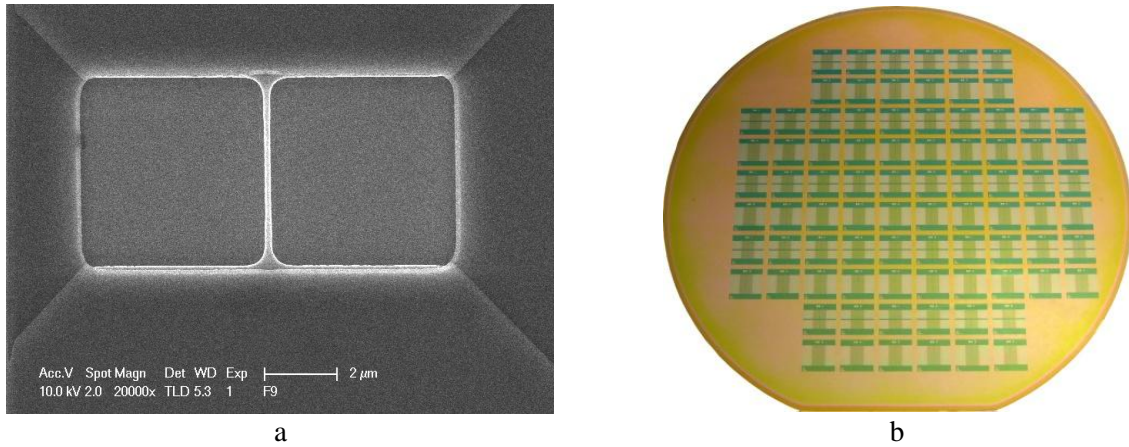


Fig. 8 a) Scanning electron microscopy (SEM) image of a nanowire device. Visible is the nanowire (center) and the source (top) and drain (bottom) terminals. The opening in the silicon nitride passivation is also clearly visible. b) Picture of a processed wafer containing 84 devices.

In this process silicon dioxide was used, but other oxides are possible as well. A new layer of resist is deposited to protect the devices during the etching while defining the contact holes (Fig. 7o-q). Deposition of aluminum follows this step, creating the contact leads (Fig. 7r). After the lift off process, a final sintering step is performed to ensure good ohmic contacts. Eventually the wafer (Fig. 8b) can be diced to separate the individual dies, enabling characterization in gaseous or fluidic environment [16]. In Fig. 8a and Fig. 9 images are shown of a fabricated nanowire device.

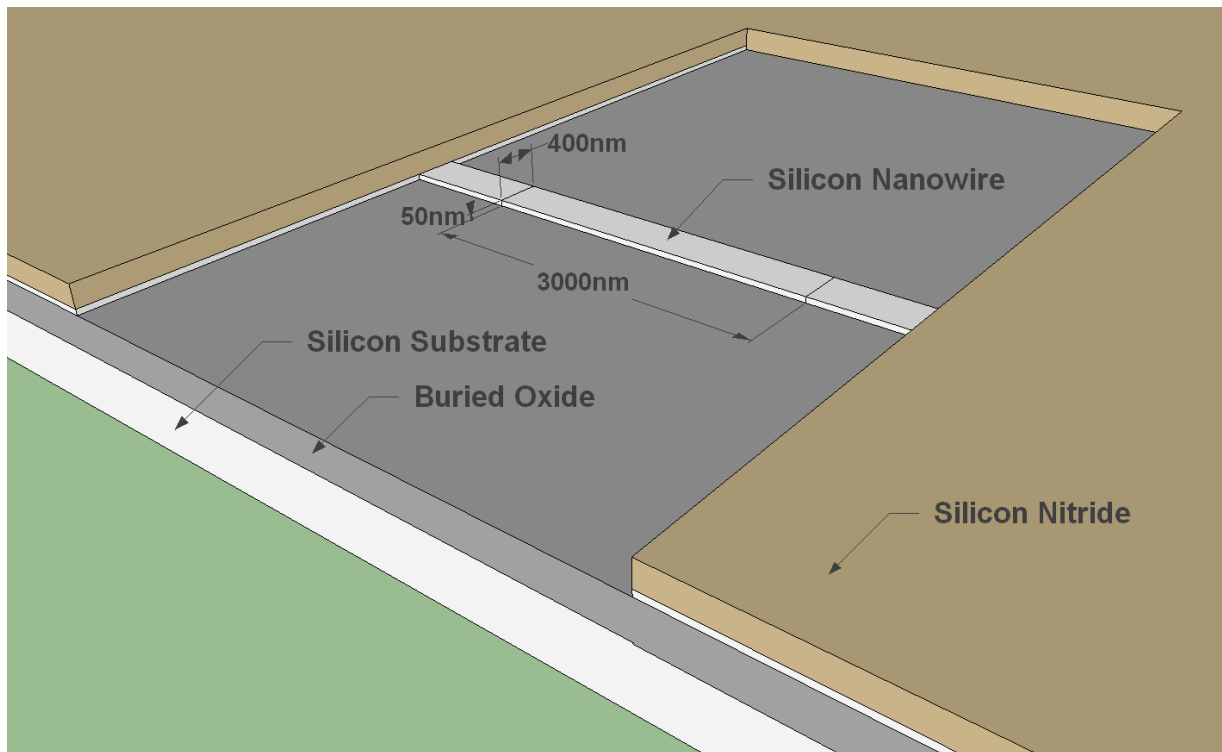


Fig. 9 3D illustration of a silicon nanowire with a cross-section through the device, showing the BOX and substrate layer.

4 Measurement Methodology

This chapter describes the method that is applied to characterize the samples. Primarily used equipment is listed and their use is described. The parameter extraction from the measured data is also discussed.

4.1 Setup

The equipment used for the characterization of the nanowires is shown in Fig. 10. The electrical characterization was done using a Keithley Model 4200 Semiconductor Characterization System equipped with seven source measurement units (SMUs) and preamplifiers. An identical system with three SMUs (Fig. 11a) was used for the characterization of samples selected for wirebonding.

The initial characterization and selection of samples (Fig. 11b) is carried out on a Cascade Microtech probe station. These samples are subsequently attached with electrically conductive glue to a chip carrier and wirebonded. Four devices are wirebonded: two in the top left and two in the bottom left as seen on the layout of Fig. 6a. After this step the microfluidic components are added on top. With most experiments this involved a polyester sealing, microfluidic cap, and silicone tubing, as described in chapter 5. Further electrical characterization is carried out using a measurement box in a fume hood. The measurement box features a zero insertion force (ZIF) socket to hold the chip, and externally available electrical connections to the chip, providing a stable and reliable measurement platform. The chip is shielded with aluminum foil to prevent an influence of light on the measurements.

The liquids are pumped through the microfluidics and over the sample surface by a Harvard Pump 33. This pump is equipped with two identical Hamilton glass syringes with a volume of 50 mL. Switching between these liquids is done manually by changing the tubing connections.



Fig. 10 Photographs showing the measurement setup: a) the fume hood with cables coming in from the Keithley 4200 SCS, b) the pump on the left, and measurement box in the center with a sample.

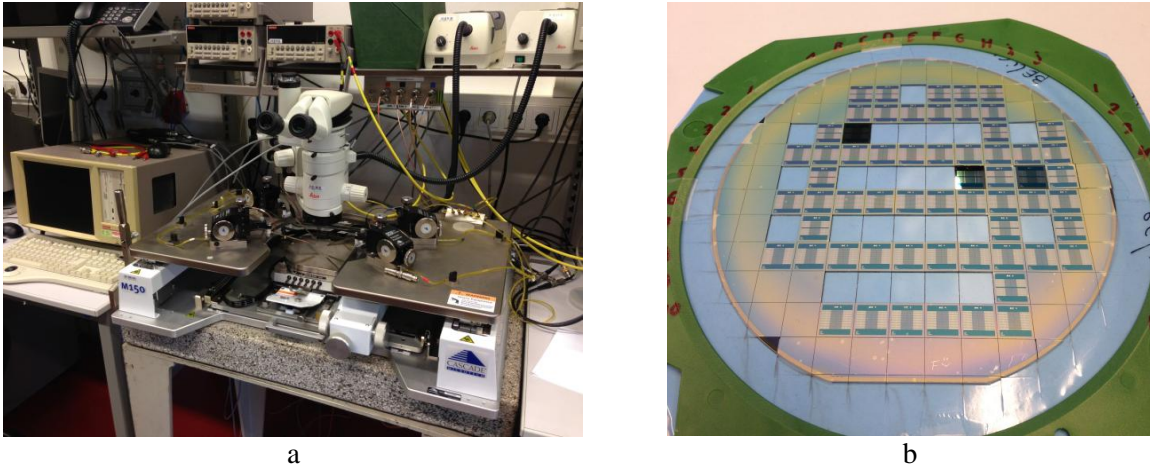


Fig. 11 Photo of a) the Cascade Microtech probe station and the Keithley 4200 SCS b) diced wafer with most of the silicon nanowire devices still covered with dicing foil.

4.2 Settings

The characterization of samples selected for wirebonding is done by applying a known potential on the gate, drain and source contacts and measuring the drain current. One SMU is connected to the chuck and provides the backgate voltage, while two other SMUs contact the drain and source contact of a nanowire device. The devices are electrically connected as shown in the schematic of Fig. 12. The drain and source voltages are respectively 50 and 0 mV and are applied continuously during the measurement. The gate voltage is swept from high to low, and is pulsed. The waveform is defined by the parameters t_{on} , t_{off} and V_{base} , the range of the gate voltage to be swept through, and the increment in gate voltage. These parameters are summarized in Table 1.

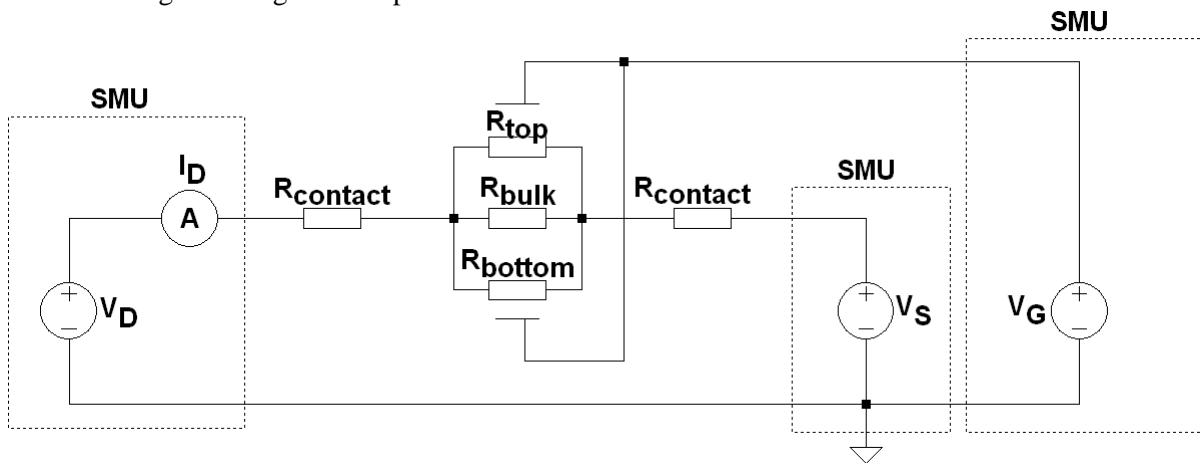


Fig. 12 Electrical schematic showing how a single device is connected to the measurement system through the use of three source measurement units (SMUs).

The characterization of samples in a liquid environment is done in a similar way. Except now it also includes a set amount of time before each sweep where all drain, source and gate potentials are held equal to a constant voltage. This amount of time was 8 seconds and was executed using the sampling mode. The exact value of the voltage depends on the specific experiment. The purpose is to ensure equal starting conditions among the measurements. Another difference is that now three devices are measured in parallel. One SMU is connected to the common backgate while the other six form three identical pairs, connecting to the drain and source of three separate devices. The measurement (including the equalization) is typically repeated for 5 or 10 times. One repetition is referred to as a cycle. The measurement parameters for the drain and source SMUs are identical to

those listed in Table 1. The parameters for the gate vary depending on the experiment. All measurements were performed with speed set to ‘normal’ which has a delay and filter factor of one and automatically determines the A/D aperture time.

	SMU1 / Drain	SMU2 / Source	SMU3 / Gate
Voltage [V]	0.05	0	0 to -12
Voltage step [V]	-	-	-0.02
Voltage range [V]	0.2	0.2	20
Current range [A]	1E-6	1E-6	10E-9
Current compliance [A]	1.05E-6	1.05E-6	1.1E-9
Pulsed settings	-	-	$t_{on} = 5 \text{ ms}$ $t_{off} = 10 \text{ ms}$ $V_{base} = 3 \text{ V}$

Table 1 Keithley 4200 SCS settings for selection of samples. The settings used during characterization in liquids are identical for the source and drain SMUs, but vary for the gate SMU depending on the specific experiment.

A pulsed-mode measurement is used to apply the gate voltage. The waveform is shown in Fig. 13a. The sequence consists of an ‘on’-pulse of which the length in time is defined by t_{pulse} which is the sum of t_{on} and $t_{measure}$, and an ‘off’-pulse defined completely by t_{off} [17], [18]. The value of $t_{measure}$ is determined by the slowest measurement that has to be performed. The voltage applied during the on-pulse is the gate voltage and during this time the drain current is measured. The voltage applied during the off-pulse is the so-called base voltage V_{base} . The purpose of the off-pulse is that the net voltage applied over the course of the measurement can be made equal to zero. This will result in a constant effect on the ions in the solution and promotes a stable measurement [18]. This is not the case when the gate voltage is swept as a stepped waveform as shown in Fig. 13b. This is referred to as a continuous- or constant-mode. Unless the range is symmetrical around 0V, such a waveform will result in a net non-zero voltage.

Another effect of the measurement system is the initial application of two relatively long pulses with a value of first V_{base} and subsequently the initial value of V_{gate} before the start of the actual series of measurements [17].

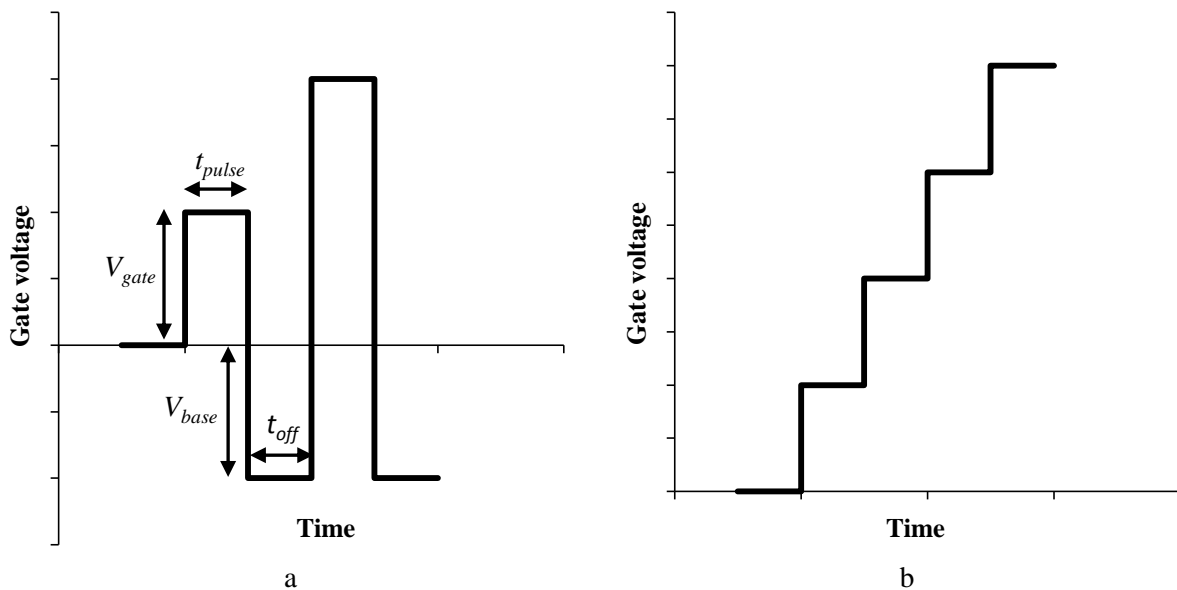


Fig. 13 Plots showing the a) pulsed waveform and b) continuous waveform.

The pump settings are defined by syringe diameter and flow rate. The syringe diameter is 32.6 mm. The pump is turned on for a certain amount of time to refresh or replace the liquid on the sensor

and then turned off before measurements take place. The flow rate typically used ranges from 0.05 to 0.2 mL/min.

4.3 Measurement Artifacts

4.3.1 Measurement System

The Keithley 4200 SCS comprising eight SMUs has been used to electrically characterize the silicon nanowire devices. The initial method used to measure the drain current of these devices resulted in artifacts showing up in the measurements as shown in Fig. 14a. This measurement involved a pulsed-mode sweep of the gate voltage. The drain current levels observed prior to the jumps are listed in Table 2. This initial method uses a setting called ‘limited auto’ for the SMUs that measure the drain currents. This means it can freely switch between current ranges to minimize the measurement error, but staying above a specific lower limit (here 100 pA). Another observation of a measurement artifact is shown in Fig. 14b. This measurement involved a constant-mode sweep of the gate voltage. The characteristic of device 1 and 2 shows significant simultaneous changes. It is very likely that this is caused by the machine changing current measuring ranges, which is confirmed by the SMU status codes. The artifact in Fig. 14b actually more closely coincides with the source instead of the drain current range change of device 3. The source current value is -51.5 pA prior to the change and the SMU status code reads as 001C0020. For the next voltage step the current value is -93.4 pA and the SMU status code reads as 001C0030.

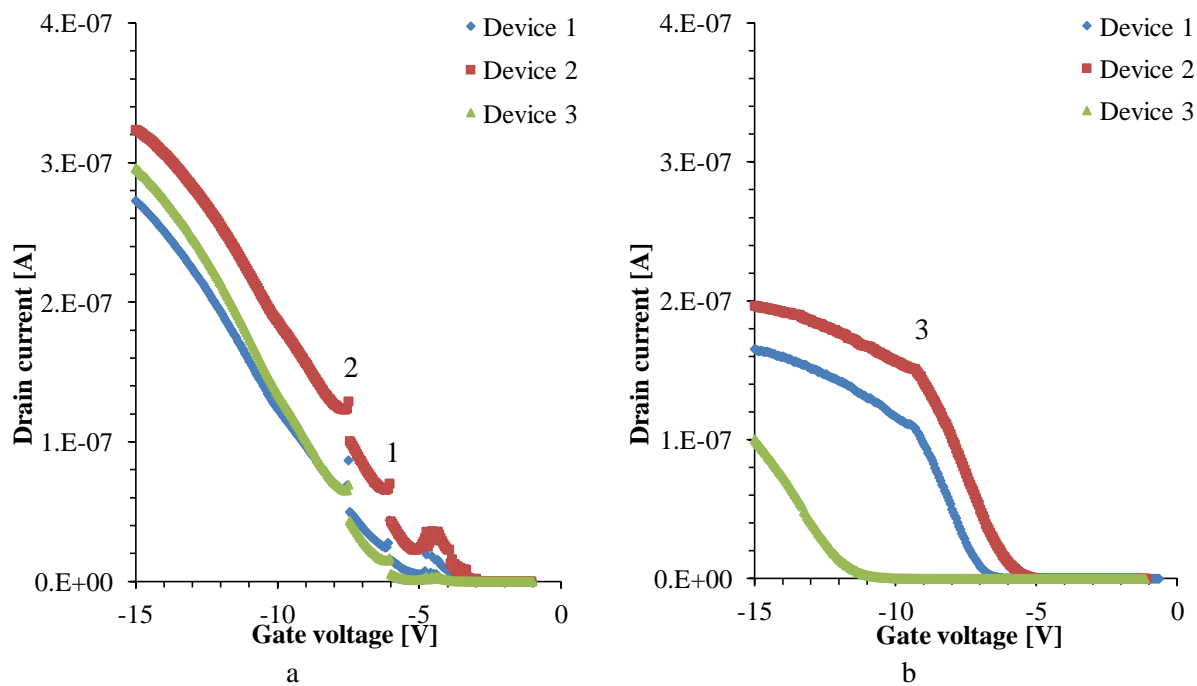


Fig. 14 Two measurements from chip W2C7. The distinct artifacts have been labeled. a) a pulsed-mode gate sweep, b) a constant-mode gate sweep.

Device	Drain current at step 1 [nA]	Drain current at step 2 [nA]	Drain current at step 3 [nA]		
1	15.05	49.78	98.64		
2	43.02	100.50	143.20		
3	5.30	43.39	47.47E-3		

Table 2 The drain currents directly before the measuring artifacts occur as shown in Fig. 14.

These measurement artifacts hamper the reliable extraction of the slope parameter, and appear to change the measured device characteristic as well. A solution to this was found by setting the current measurement range to a fixed range. This fixed range should be larger than the maximum drain current. A fixed current range of 1 μA was used for the drain and source SMUs.

However, now a new measurement artifact appeared. As shown in Fig. 15a the artifact occurs whenever the last device reaches a drain current of 80 nA, which affects all measured device characteristics. It was found that decreasing the gate current compliance decreased the magnitude of this artifact, ultimately disappearing for 1.1 nA as shown in Fig. 15b. Both measurements are performed with a fixed gate current range of 10nA. Similarly, when the gate current range was decreased from 10 nA to 1 nA, and subsequently the associated current compliance, similar results were obtained. Fig. 16 shows the transconductance plot of device 1 (Fig. 15) for a gate current compliance of 10.5 nA and 1.1 nA. Decreasing the compliance was also found to decrease the measured gate current. Unfortunately, this method did not always work. Furthermore, it was found that the gate current increases substantially when measuring the devices in a liquid environment, which rendered this method unusable, as the gate current would exceed the compliance. The measurement system will prevent a current from flowing that exceeds this compliance value.

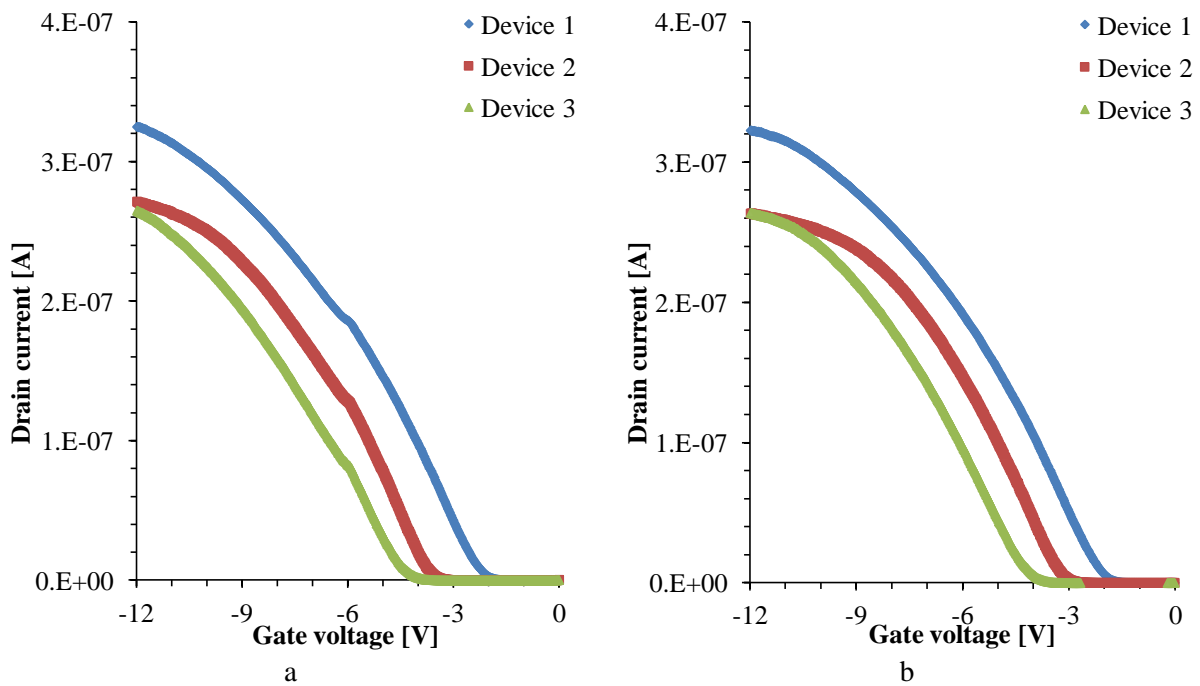


Fig. 15 Measured I_D - V_G characteristic of three devices where the gate is swept in pulsed-mode, with a fixed current range of 10 nA and a compliance of: a) 10.5nA, b) 1.1 nA. Note that the measurement artifact disappears for the lower compliance value.

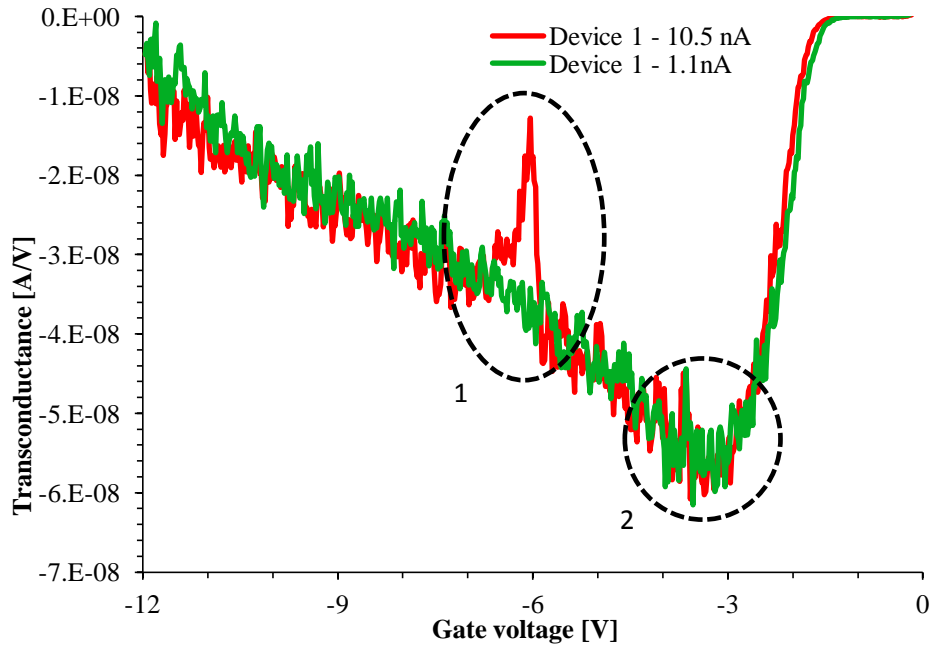


Fig. 16 Plot of the transconductance of device 1 for the case of a gate current compliance of 10.5 nA (red) and 1.1 nA (green) for a fixed current range of 10 nA. Area 1 shows how the measuring artifact affects the transconductance. Area 2 shows the area of interest, where the minimum g_m is extracted.

Another solution to this problem is found with the observation that this artifact occurs when the last device's drain current reaches 80 nA. This can be avoided by decreasing the drain-source voltage for one device in such a way that its drain current will not exceed 80 nA. The results of this method are shown in Fig. 17. However, this method also does not always work reliably.

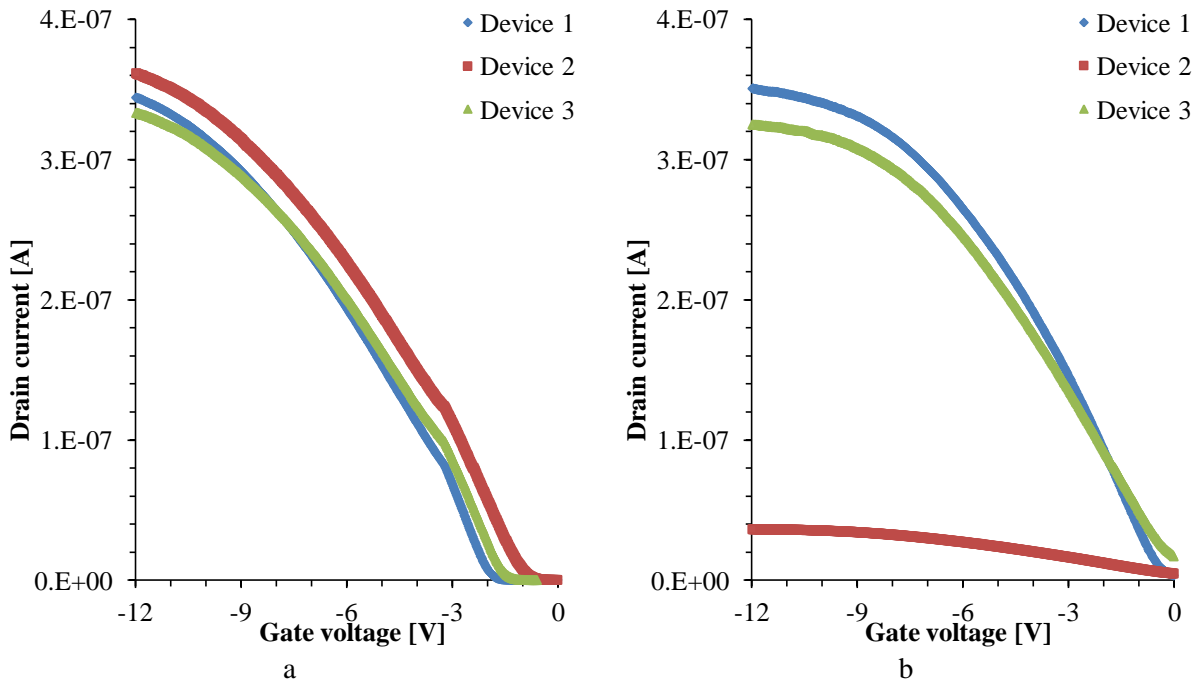


Fig. 17 Measured I_D - V_G characteristic of chip W2A5 of three devices where the gate is swept in pulsed-mode, with a fixed current range of 10 nA and a compliance of 10.5 nA: a) $V_D = 50$ mV for all three devices, b) $V_D = 5$ mV for device 2, and 50 mV for the others.

4.3.2 Handling

Before and during an experiment the chip and connected tubing has to be handled. For example, the chip has to be clamped in the setup, and the tubing has to be handled for a different liquid to be pumped. It was observed that this can have a significant influence on the measured characteristics of the devices. It is therefore essential to minimize the amount of handling that is required before and especially during an experiment.

4.3.3 Measurement Settings

It has been observed that the device characteristic is dependent on the measurement settings such as the selected scanning range for the gate voltage [18]. It is therefore critically important to keep the measurement settings constant during an experiment in order to compare results.

4.4 Parameter Extraction

The V_G - I_D characteristic of a nanowire sensor (see Fig. 18 for example) is determined by the properties of the device and its surrounding environment. The measured characteristic therefore holds potential information that could be used to sense these properties. However, comparing these characteristics will lead to a complex puzzle as there may be more variables of significance that cannot be measured or controlled. A typical solution is to narrow down the data to a form where the influence of the variable of interest is strongest and that of the other variables is minimized. This technique is referred to as parameter extraction. In this research it is the aim to find a quantifiable relation between the properties of the nanowire and that of the surrounding environment.

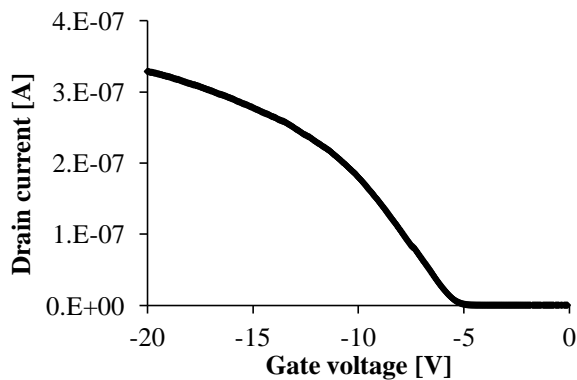


Fig. 18 Typical V_G - I_D characteristic of a p-type nanowire device. Note the gate voltage where the device appears to 'turn on', and the variation in the slope.

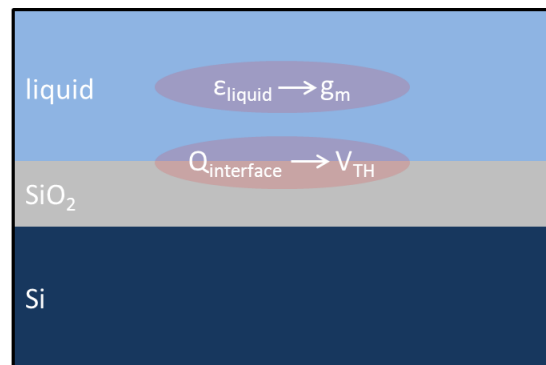


Fig. 19 Cross-section of a nanowire. Shown are the physical locations of the material properties and their theoretical influence on the electrical properties of the nanowire.

According to the theory, discussed in chapter 2, the slope of the V_G - I_D characteristic for a nanowire sensor depends on the dielectric constant between the gate and the channel. Extracting the minimum value of the slope should therefore be a promising sensing mechanism for the change in the dielectric constant of the surrounding environment. Another parameter that was extracted is the threshold voltage. In accordance with the theory this parameter can give information on the chemical state of the interface between the channel's silicon oxide and surrounding liquid environment. The location of the two abovementioned properties and the electrical parameters they influence are illustrated in Fig. 19.

4.4.1 Threshold Voltage

The term threshold voltage, or V_{TH} , originates from the context of a MOSFET. It is defined as the gate voltage where an inversion layer forms near the interface of the insulating layer and the substrate of the transistor. Starting at this voltage a significant amount of current can flow from the drain to

source contact, resembling a threshold value. A similar behavior can be observed in the operation of a nanowire, which is described using the same term. However, there is no inversion layer in these nanowires as they are used in accumulation mode.

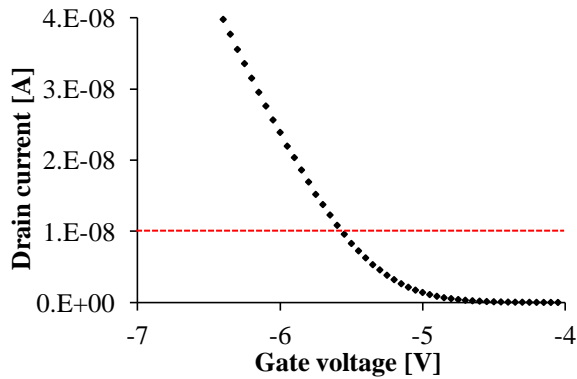


Fig. 20 Detail of Fig. 18 showing the extraction of the threshold voltage based on current level.

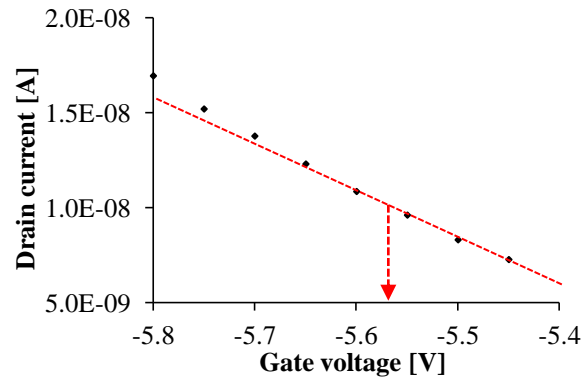


Fig. 21 Detail of Fig. 20 illustrating the linear interpolation between the closest data points around 10nA and extraction of the threshold voltage.

There are many methods that propose their own definition of the threshold voltage based upon parameter extraction from the electrical characteristic. The simplest extraction method defines the threshold voltage as the voltage for which a specific current is flowing. This method is applied in this research and is illustrated in Fig. 20. This is done by finding the closest data point above and below a drain current of 10nA and applying linear interpolation to find the voltage that matches with 10nA, as shown in Fig. 21.

4.4.2 Transconductance

The slope of the V_G - I_D characteristic is also referred to as the transconductance or g_m . Based on the theory as set out in chapter 2 it is predicted that the dielectric constant of the material in between the gate and channel will influence the slope. In order to quantify this influence the minimum slope is extracted.

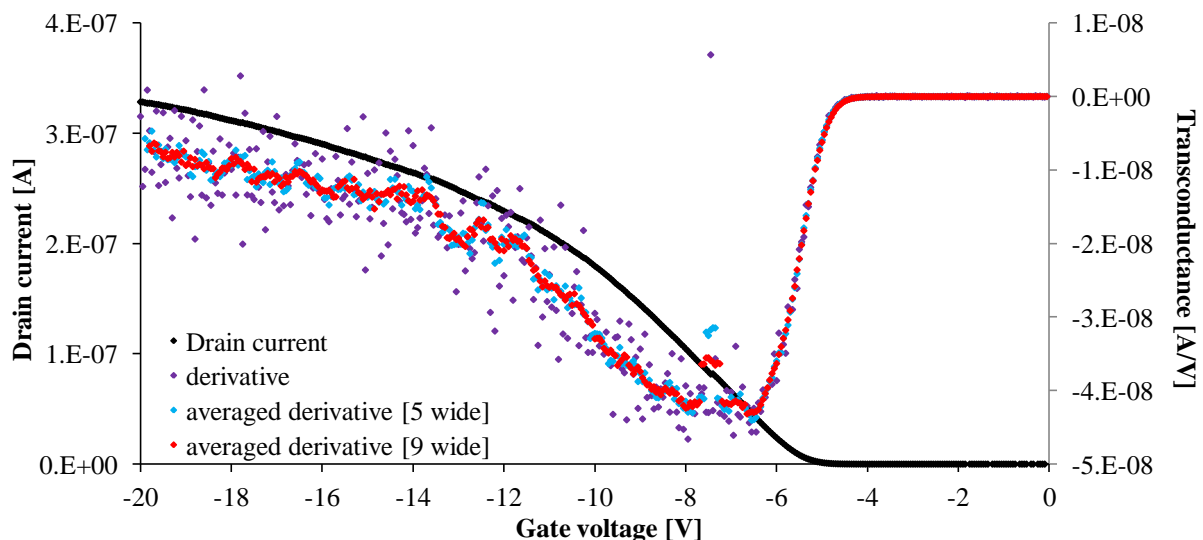


Fig. 22 Plot showing the V_G - I_D characteristic of a nanowire and the derivative of I_D with respect to V_G . Also shown is the centered moving average with a width of 5 and 9.

To calculate the slope the difference in drain current is divided by the difference in gate voltage between each data point and the next. Then the values for the slope are averaged by a centered moving average with a width of 5 data points (see Fig. 24). This is done to filter out noise. Choosing a

width for the moving average involves a trade-off between the presence of noise (precision) and the true value (accuracy). Finally, the minimum value is extracted.

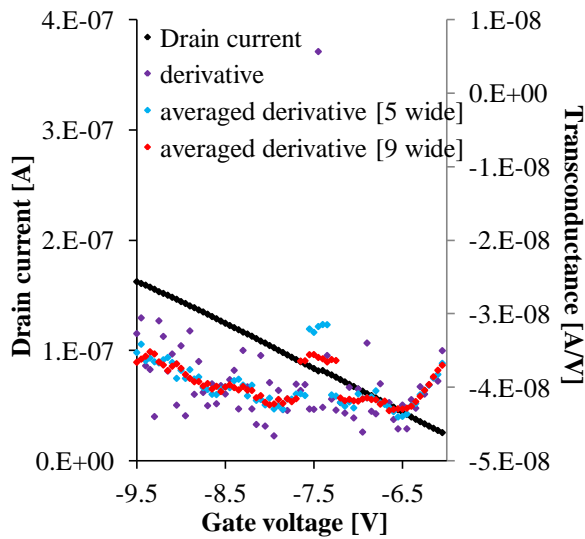


Fig. 23 Detail of Fig. 22 showing the minimum slope valley. Note the effect of the Keithley system offset error on the derivative and the moving average.

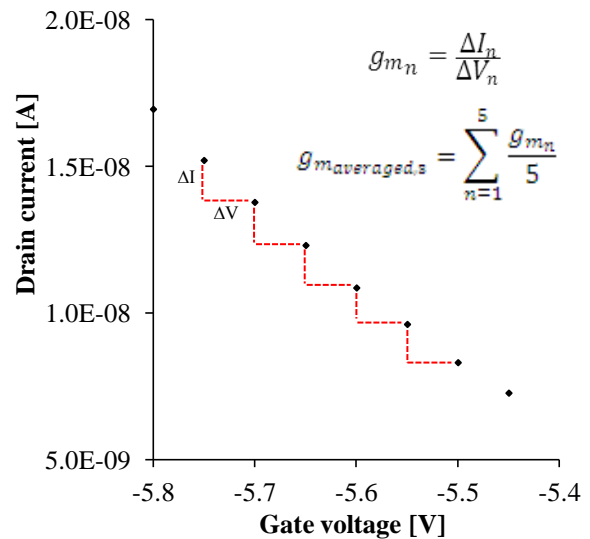


Fig. 24 Illustration of the calculation of the centered moving average with a width of 5 data points.

In this parameter extraction the offset error between the different current measurement ranges in the Keithley system becomes especially apparent, as is shown in Fig. 23. In this situation the error does not create a problem with the determination of the minimum slope as it is not in the center of the valley. Should this be the case however, one solution is to ignore the single outlying slope data point in the calculation of the centered moving average. Another solution is to change the V_{DS} of the measurements to shift this error away from the minimum as it always occurs near the crossing of 80 nA.

4.5 Conclusion

A reliable measurement setup has been established to characterize nanowire sensors in various environments. In combination with this setup a measurement protocol has been developed which defines measurement programs and their settings.

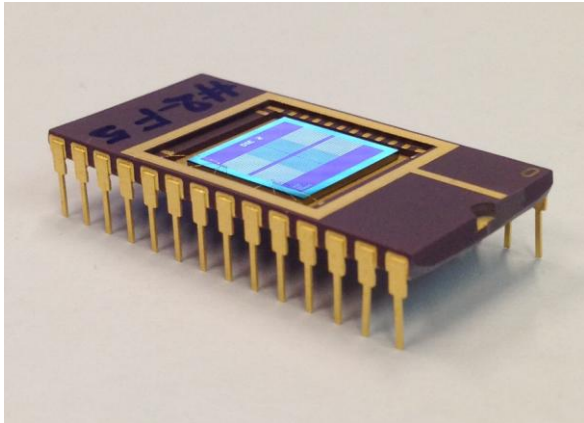
Possible error sources have been identified and solutions have been implemented. Of particular importance were the measurement artifacts originating from the Keithley measurement system.

Based on the theory of the nanowire field-effect sensor two relevant parameters have been identified for measuring the dielectric constant of liquids: the threshold voltage, and transconductance. Methods have been successfully developed in order to extract these parameters from the measurement data.

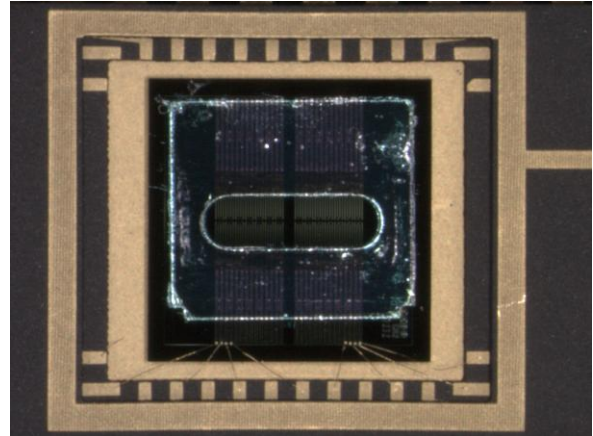
5 Liquid Interfacing

This chapter discusses the five components of the fluidic system. The aim of the fluidic system is to provide a way to introduce liquids to the devices on the chip. This should be done while preventing leaks from happening as these cause 1) bad electrical measurements 2) instability due to flow on the chip surface 3) unpractical situations when working with dangerous liquids.

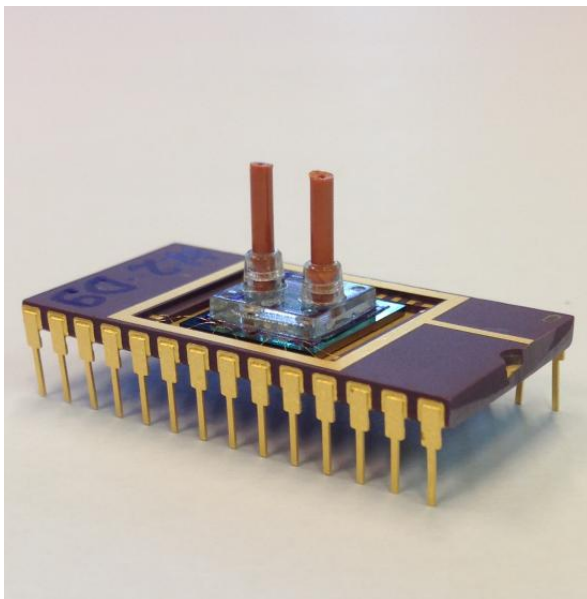
The steps required to interface the chip are illustrated in Fig. 25. Each of the following sections describes a component of this fluidic system and discusses the available options, and specific merits and problems.



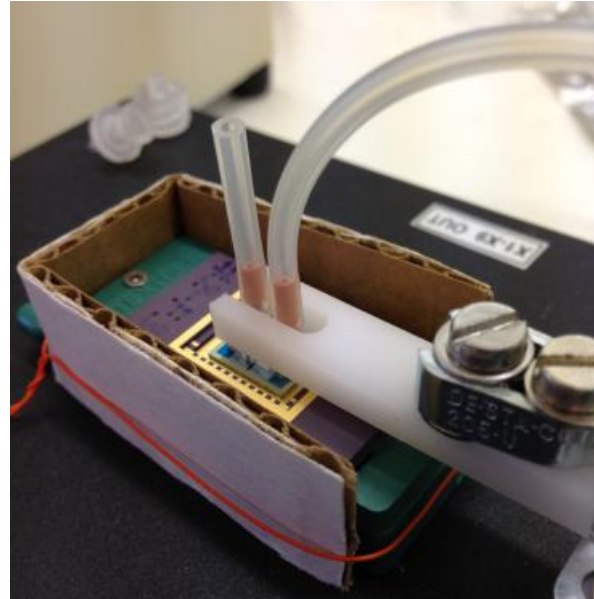
a



b



c



d



Fig. 25 Photographs illustrating the process of interfacing a chip with a fluidic system: a) first a bare die is glued to a chip carrier and device connections are wirebonded. b) then a sealing layer is aligned and attached on top of this die. c) next a microfluidic cap is put on top of this sealing layer, d) then tubing is attached to the cap and the sample is clamped in the measurement box. The cardboard serves as a spacer, preventing electrical short-circuits when e) aluminum foil is used to shield the device from light. f) Finally, the tubing is connected to the syringes in the pump.

5.1 Microfluidic Cap

The purpose of the microfluidic cap is to form a channel directly on top of the devices for the fluid to flow across the chip. The shape and sizes can be seen in Fig. 26. The narrow side at the far end of the channel is the weakest point and leakage often occurred at that location. This is due to the difficulty with the lever-type clamp to apply even pressure across the cap. This was solved by adding a sealing layer that is positioned between the microfluidic cap and chip.

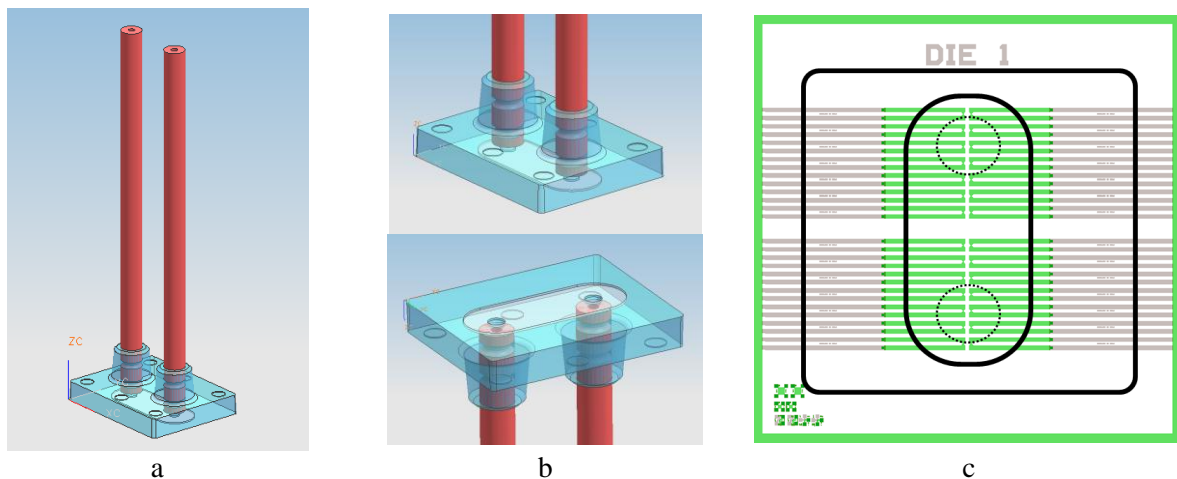


Fig. 26 a) the microfluidic cap b) detail showing the channel. The channel is 3mm wide and 8 mm long (at their maximum) and is 0.1mm deep [19] c) the footprint of the microfluidic on the chip. The black lines denote the edges of the microfluidic. The dotted circles denote the in- and outlet port.

5.2 Liquids

Two liquids were used to create mixtures with a range of dielectric constants. The first liquid is demi-water with a dielectric constant of 80, a density of 1.00 g/cm^3 . The other liquid is 1,4-dioxane (see Fig. 27), also referred to as dioxane, with a dielectric constant of 2, a density of 1.03 g/cm^3 . All

properties are at room temperature. These liquids are miscible (mix in all proportions) and the dielectric constant of a mixture varies according to weight percent dioxane as shown in Fig. 28.

5.2.1 Residue

Dioxane, being an organic solvent, was the cause of many issues in the experimental setup. One problem was likely caused by dioxane and resulted in visible deposition (see Fig. 29) of an unknown substance on the chip surface. The hypothesis is that dioxane dissolves small amounts of the silicone tubing or microfluidics, as these components were present in all cases where this deposition was observed.

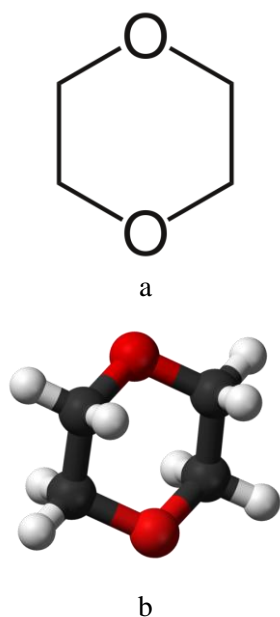


Fig. 27 a) chemical structure of 1,4-dioxane ($C_4H_8O_2$), b) ball and stick model of 1,4-dioxane.

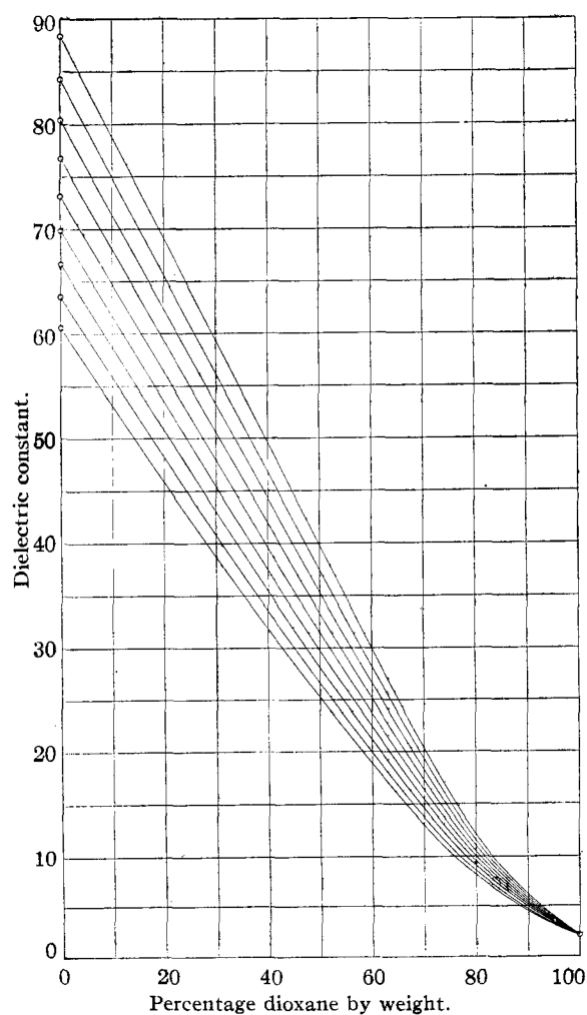


Fig. 28 Curves for the isotherms of the dielectric constant of dioxane-water mixtures of varying composition: top curve is the 0°C isotherm, then follow in order those for 10, 20, 30, 40, 50, 60, 70 and 80°C. As measured at a frequency of 2MHz using a resonance method. Graph reproduced from [20].

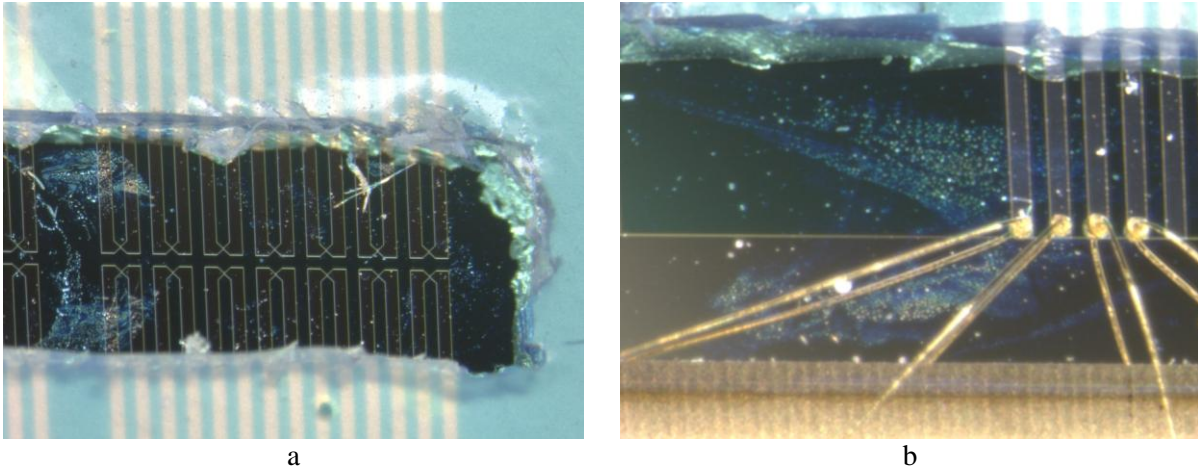


Fig. 29 Optical photographs from a sample with a SIFEL sealing layer after an experiment involving demi-water and dioxane. a) shows typical visible signs of deposition (the circle on the left is from evaporation after opening the chip, but right side shows typical observation) b) dioxane has leaked out and evaporated, leaving residue behind. This has also been observed with a silicone and polyester sealing layer.

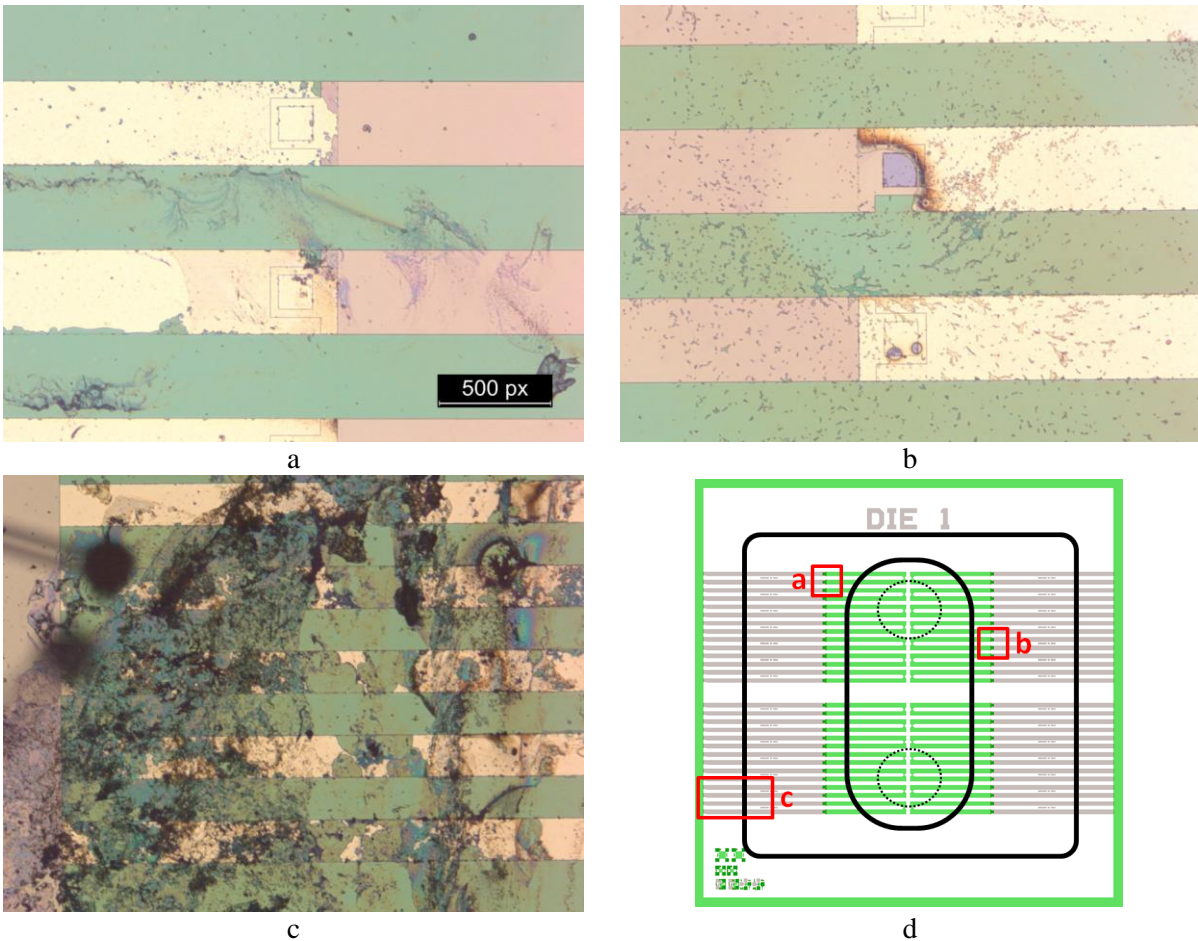


Fig. 30 Optical photographs from two separate samples. a) corrosion of aluminum due to prolonged demi-water exposure b) corrosion due to exposure to a 0.1M KCl aqueous solution revealing the via structure c) and on the same sample extensive corrosion of the aluminum contacts, even causing the bondwires to detach (top left). d) approximate location of the photographs on their samples.

Another possible cause is precipitation of 2,6-di-tert-butyl-4-methylphenol, which is a stabilizer added to dioxane at 25 ppm. Precipitation occurs under the influence of light and the presence of oxygen. For this reason the dioxane was stored in a dark environment and bubbled with nitrogen gas for at least 30 minutes before use to drive out oxygen.

In order to avoid the problems associated with dioxane the use of another liquid was considered, but this option was not explored exhaustively. Since a suitable replacement of dioxane is likely to be found in another organic solvent (such as isopropanol), because the liquid should be miscible in water. This will lead to similar problems.

5.2.2 Ion Solubility

Another issue is the low solubility of KCl in pure dioxane, or a 90/10 (volume %) dioxane/water mixture. Adding KCl to the mixture as a solid or as a solution in water did not make a difference, in both cases KCl does not dissolve. This didn't allow for spiking the mixture with a known ion concentration (0.01M), which can be explained through dioxane's nonpolar character which makes it energetically unfavorable for KCl to dissociate. This has an important consequence for when dioxane is introduced to the device surface. For the silanol groups it is less energetically favorable to deprotonate in dioxane compared to water, for this reason. Based on the results of the pK_a of acetic acid in water-dioxane mixtures [21] the pK_a of the silanol groups is therefore expected to increase in dioxane.

5.2.3 Aluminum Corrosion

The corrosion of the aluminum contacts and vias forms another issue, when contacted to demi-water. In general it can be said that the purer (lower ion concentration) the water, the faster the corrosion reaction. Aluminum is known to be highly resistant to corrosion, but the chemical stability of the oxide film can be compromised depending on the local pH value of the environment. Exposure to demi-water for 20 hours has resulted in poor electrical connections (see Fig. 30). On top of this, chlorine ions present in the solution, or the fluidic materials, act as catalyst. Initially three solutions were applied simultaneously to avoid this problem: 1) do not leave demi-water in the system when it is not in use, but flush it with air, 2) do not use KCl spiked solutions, 3) place the fluidic system in such a manner that the aluminum belonging to the devices that are being measured, is further away from the fluid channel (in Fig. 30d, by moving the fluidic footprint shown in black to the right, as devices on the left are used), decreasing exposure and increasing the lifetime.

5.3 Tubing

The tubing connects the syringe with the fluid to the inlet of the microfluidic. Another piece of tubing connects to the outlet and allows for the fluid to exit to a waste container. The ideal tubing has the following properties: 1) transparency, in order to detect the different fluids in the system and notice any leakage or clogging problems in an early stage 2) chemical resistance, so it does not contaminate the fluid or weaken to the point of failure 3) flexible, making it practical to work with, and not mechanically stress the microfluidic 4) matching size. If the inner diameter of the tubing is slightly smaller than the tubing on the microfluidic, then it can be fitted without the use of connectors, preventing a weak point with respect to leakage.

Several tubing types have been investigated. Silicone tubing is transparent, flexible, and readily available with the right sizes. It does however weaken slightly when exposed to dioxane, but this has not led to leakage. Silicone tubing has therefore been the most used type of tubing. Tygon tubing has similar properties as silicone, but showed significant mechanical weakening and white discoloration upon exposure to dioxane. PFA and FEP tubing is transparent and chemically resistant, but not as flexible as silicone tubing. This is problematic when trying to fit the tubing in a reliable and leaktight manner, requiring the use of a connector.

5.4 Connectors

In this report a connector is used as a broad term to include all methods to mechanically bring two pieces of tubing together in a reliable and leaktight manner. The connection between the syringe and the first piece of tubing is made with plastic luer-lock connectors (Fig. 31a). These have not shown any sign of chemical attack due to dioxane, are convenient for repeated (un)coupling, and are leaktight. This method is also used to connect to the smaller piece of tubing leading to the tubing of the microfluidic. This works best when the tubing is flexible so that it can be fitted on the luer-lock connectors without the need for extra measures to make it leaktight (Fig. 31b). This is particularly important as these extra measures have their own specific problems. Two methods have been tried with tubing that did not have a suitable inner diameter to create a leaktight fit. The first is a zero dead volume connector (Fig. 31c). Although this connector is leaktight, it is also too big to fit and creates stress on the microfluidic. This becomes a bigger problem when tubing has to be switched (for a different fluid) requiring handling. Another method is to use the luer-lock connectors with heatshrink wrap, although this often led to leakage or mechanical failure (Fig. 31d).

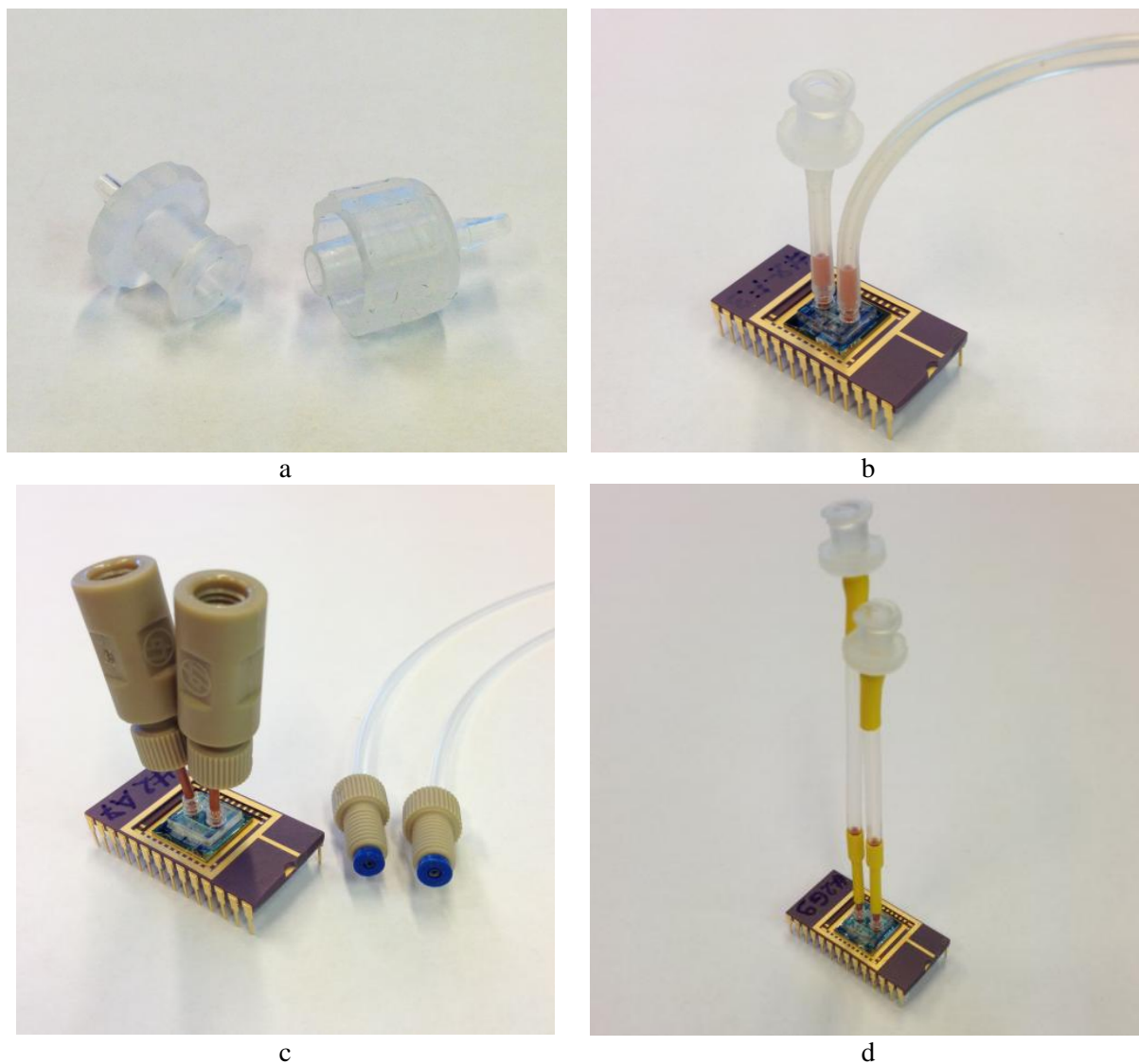


Fig. 31 Four different methods to create connections: a) luer-lock connectors, b) a leak-tight fit between the microfluidic cap and tubing, c) zero dead volume connectors, d) heatshrink.

5.5 Sealing

The sealing is positioned between the microfluidic cap and the die surface. It is necessary because the microfluidic cap is rigid and will leave gaps around the perimeter giving rise to leakage. To fill these gaps, a flexible sealing layer is used as an intermediate connection. The ideal sealing layer has the following properties: 1) chemical resistance to water and dioxane, 2) electrically nonconductive, 3) flexible to fill gaps and prevent leakage, 4) does not stick so that it can be easily removed for surface characterization of the devices. Several sealing methods have been investigated.

The sticky sealing that comes already attached to the microfluidic cap is very convenient for assembly of the fluidic system as one alignment step is already taken care of (Fig. 33). Although this material is able to provide a leaktight seal for water, it is prone to leakage during dioxane exposure.

An attempt to improve upon this solution involved depositing liquid laser scribe photoresist around the perimeter for a leaktight seal (Fig. 35a). This was subsequently left to harden in a vacuum environment. Unfortunately, this solution was also prone to leakage. This is likely due to the clamping step when inserting the chip into the measurement box, cracking the hard photoresist. Omitting the clamping step is however not possible as the mechanical stress from handling the tubing can cause cracks in the photoresist or detach the microfluidic cap.

Silicone rubber is the second sealing layer that was investigated. A mixture of the polymer material and curing agent was deposited on a wafer with a Teflon coating and left to cure. From this non-sticky material a sealing layer was cut, and is able to provide a leaktight seal for water, but is not reliable with dioxane (Fig. 35b).

The third option that was explored is a double-coated tape with a thickness of 0.1mm, known as Nitto 5015P. It consists of a modified acrylic adhesive on both sides of a PET (polyester) carrier. From this material sealing shapes with alignment marks were lasercut. Three designs were made, where only the channel size was varied (Fig. 32a-b). The largest channel size matches that of the original sticky tape on the microfluidic cap (radius of 1.5mm). But because this original tape often led to leakage, smaller channel sizes were designed. Only the 1.0mm channel radius design was used in experiments and this worked excellently. The alignment marks help with assembly. Assembly is done by taking of the protective liner from one side and aligning the sealing shape with geometry on the chip (Fig. 35c-d). Then attach the sealing layer and apply pressure to ensure a good adhesion. Then remove the liner on top and align the microfluidic cap with the alignment marks. Attach the cap and again apply pressure to ensure a leaktight fit. This solution has proven itself to be leaktight with water

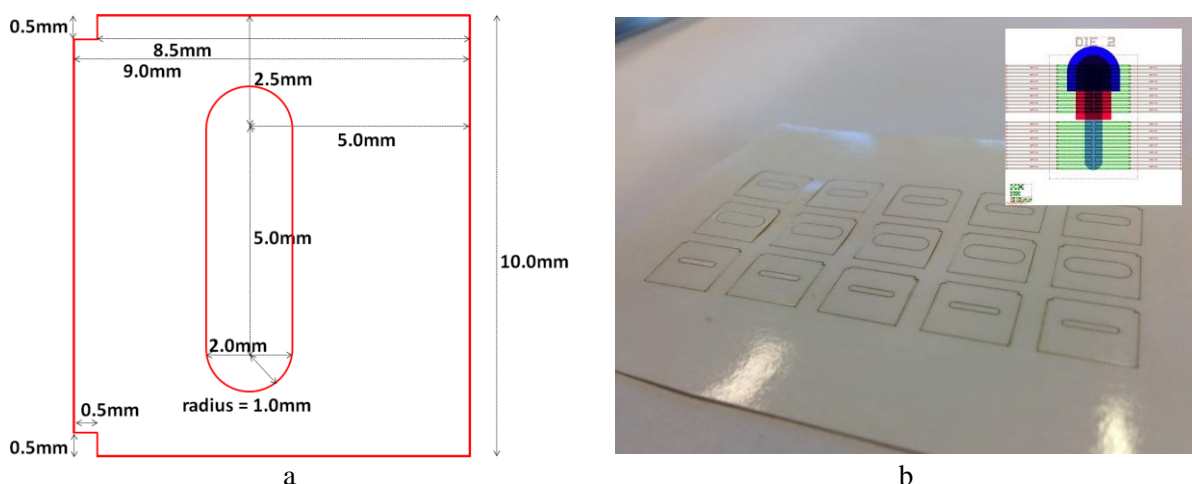


Fig. 32 Design of the polyester sealing layer: a) three designs where only the radius (and with it the width) of the channel was varied: 0.5, 1.0, and 1.5mm radius, b) these designs were lasercut from polyester sealing material. The inset shows the (partial) overlay of the channel area of the three designs on the chip.

and dioxane. However, exposure to dioxane does damage the sealing layer. Clogging has been observed to occur after prolonged exposure to dioxane, likely due to the weakening of the sealing layer (Fig. 35e).

A fourth sealing material that has been briefly investigated is a polymer called SIFEL (Fig. 34) manufactured by Shin-Etsu). This material was spincoated on a wafer and subsequently cured in a heating step. This non-sticky material holds great potential due to its excellent resistance to polar solvents (Fig. 35f).

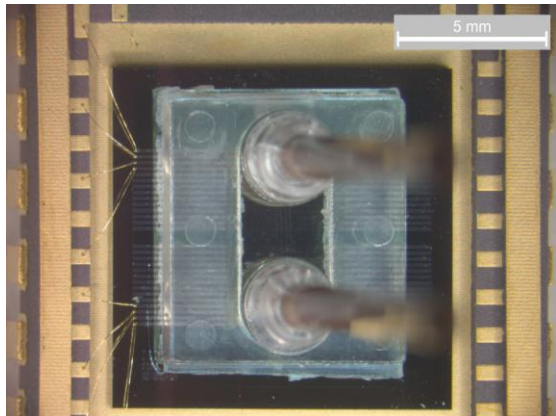


Fig. 33 Photograph showing the original sticky tape underneath the microfluidic cap. Its footprint matches the cap design.

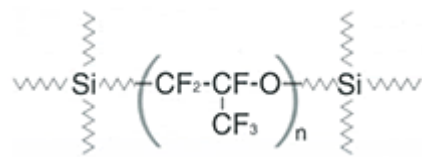
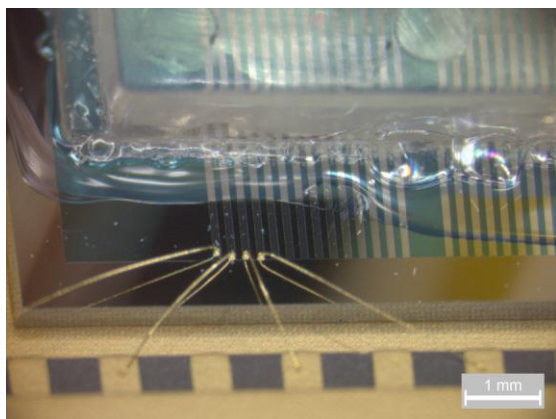
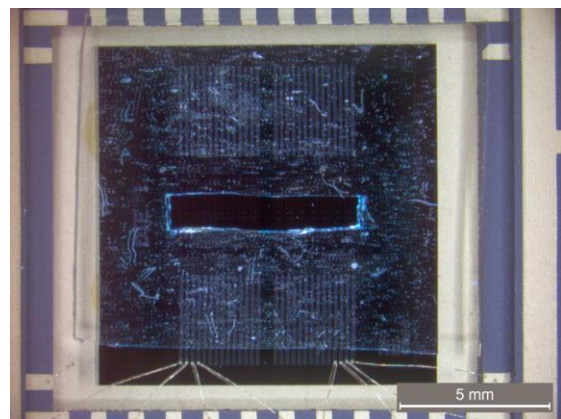


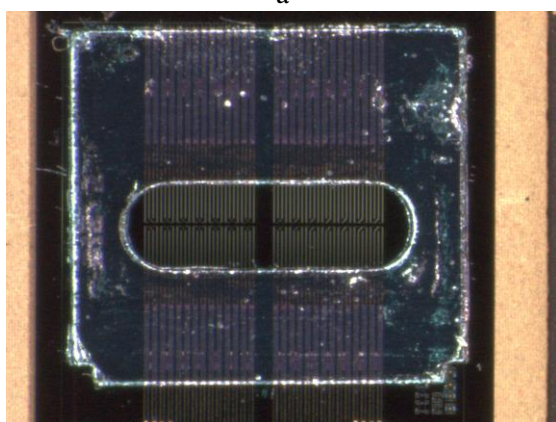
Fig. 34 The chemical structure of SIFEL, reproduced from [22].



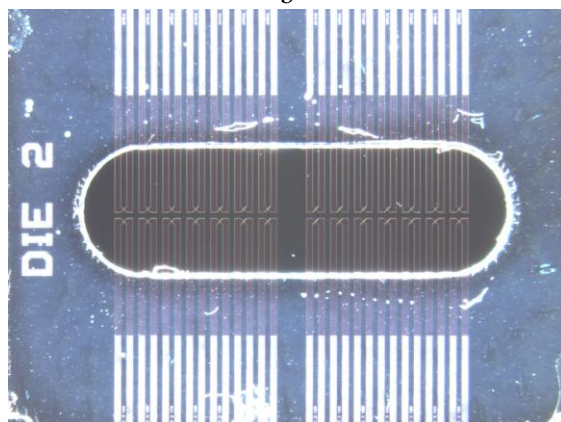
a



b



c



d

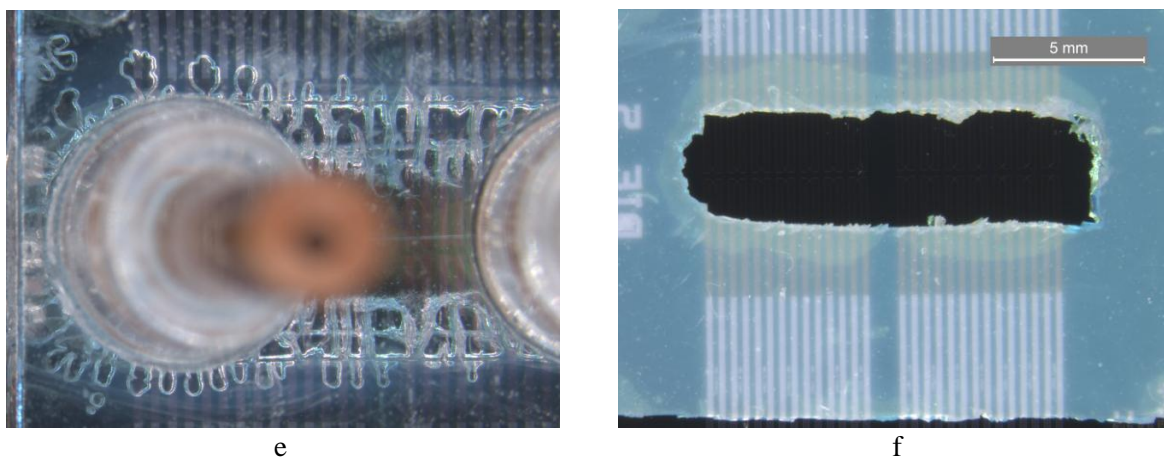


Fig. 35 Photographs showing four sealing methods: a) sealing layer with laser scribe photoresist, b) silicone rubber sealing c) polyester sealing. d) close-up of polyester sealing and channel, e) weakening of a polyester sealing layer due to prolonged exposure to dioxane, f) SIFEL sealing. Note: the scale bars are not correct.

5.6 Pump and Syringes

The liquids are pumped by a Harvard Pump 33 and is equipped with two identical Hamilton glass syringes with a volume of 50 mL. Switching between these liquids is done manually by changing the tubing connections. The flow rate typically ranges from 0.05 to 0.2 mL/min. For higher flow rates the risk of leakage increases as the pressure is higher. A lower flow rate also allows for timely intervention when leakage occurs to prevent excessive spillage.

5.7 Conclusion

Dioxane has been selected as the liquid to complement water for characterization of the nanowire sensor, due to its low dielectric constant and miscibility. However, dioxane is a strong organic solvent and was found to cause leakage with the old microfluidic setup. The microfluidic system has been analyzed and its weak points have been identified. As a result several solutions have been investigated. Finding a suitable material for the sealing layer proved to be of particular importance and difficulty. It was found that a sealing layer based on an acrylic adhesive on a polyester carrier proved sufficiently durable. In addition, silicone rubber has been identified as a suitable tubing material. These efforts resulted in a microfluidic setup that successfully contained the liquids for the duration of the experiments as reported in this research.

6 Experimental

This chapter provides a detailed discussion of the experimental results achieved with the nanowire field effect sensor when exposed to different environments, e.g. air, water, etc.

6.1 Properties in Air

The properties of the silicon nanowire devices shown below were determined in air. The first measurement results were obtained with bare dies on a probe station, while these were exposed to air and light. These measurements were performed to verify their functionality before wirebonding. Fig. 36 shows results for such a measurement from die W2F3, where four devices have been measured and compared. It is observed that the threshold voltages are negative and grouped with a difference of at most 1V. Furthermore, the drain current levels off for higher negative gate voltages and appears to saturate to a value between 300 to 400 nA. These results can be treated as typical results for bare dies.

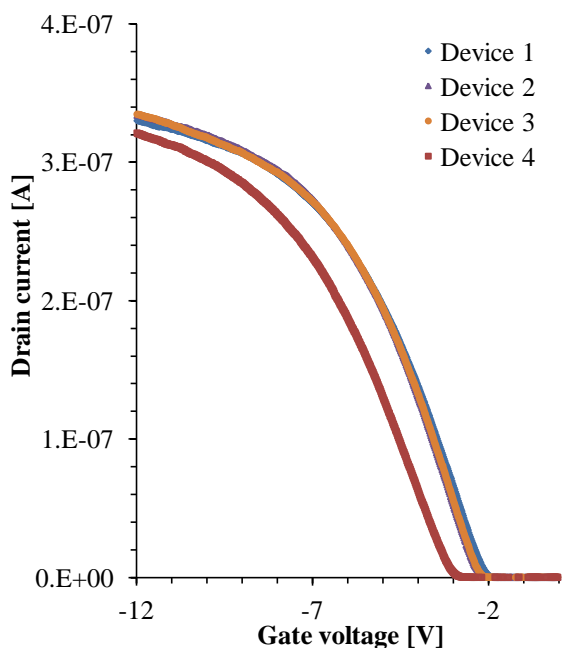


Fig. 36 Plot of I_D - V_G for four devices on die W2F3.

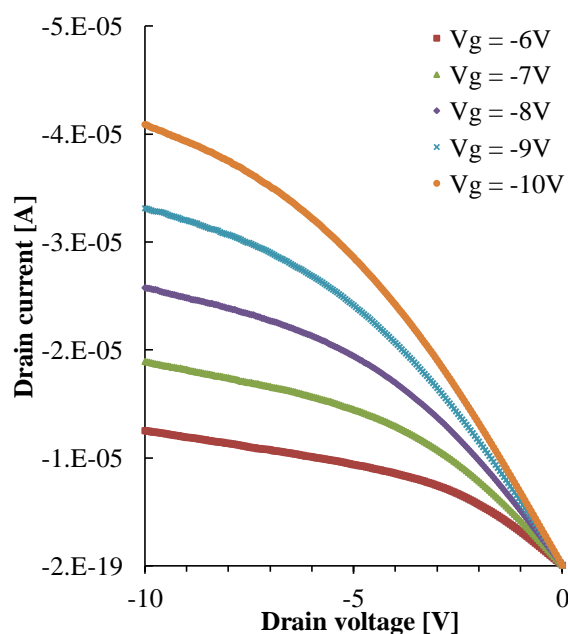


Fig. 37 Plot of I_D - V_D for different gate voltages.

The next experiment was carried out in order to investigate the leveling off of the drain current for higher negative gate voltages. This was done on a probe station, where the die was exposed to air and light. This experiment consisted of two parts. In the first part the drain current was measured as a function of drain voltage for several different gate voltages. The drain voltage range was 0 to -10V with steps of -50mV. The gate voltages used were -6 to -10V with steps of -1V.

The results in Fig. 37 show that for higher negative drain voltages the drain current levels off as well. However, our experiments use a value for the drain voltage of 50mV. As can be seen the drain current is approximately linear for these small negative voltages.

The second part of the experiment involved measuring the drain current as a function of the gate voltage, for several drain voltages. The drain voltages were 25, 50, 75 and 100mV. The gate voltage was swept from 0 to -15V. The results are shown in Fig. 38a. The drain current and minimum transconductance, g_m , have been extracted and are listed in Table 3. The results show that the saturation current and minimum g_m scale linearly with the applied drain voltage. In another measurement the gate voltage was kept constant at -10V while the drain voltage was swept from 0 to 1V and back (Fig. 38b). These results confirm that the drain current varies linearly with the applied drain voltage in accumulation mode for small drain voltages.

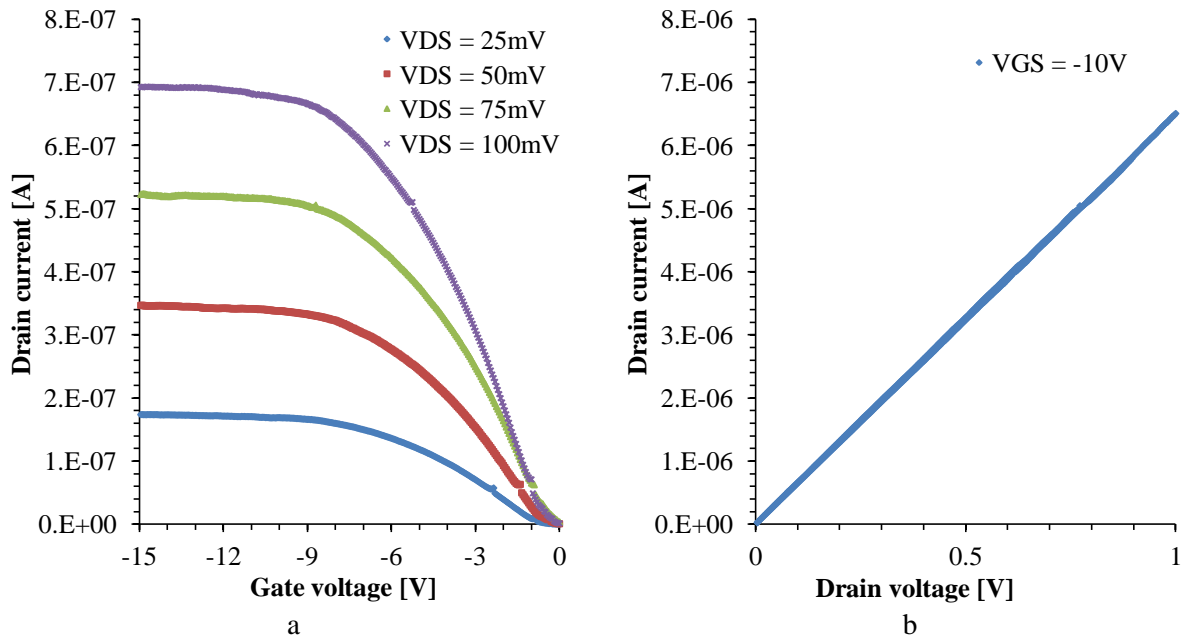


Fig. 38 Results from experiments on chip W215: a) I_D - V_G for four different values of V_D , b) dual sweep of I_D - V_D for a constant V_G .

V_D [mV]	I_D [nA] at $V_G = -15V$	I_D normalized with I_D at 100mV	Minimum g_m [nA/V]	g_m normalized with g_m at 100mV
25	173.6	0.2505	-33.04	0.2397
50	346.5	0.5001	-65.28	0.4736
75	522.5	0.7541	-105.07	0.7623
100	692.9	1.0000	-137.84	1.0000

Table 3 The drain current at two different gate voltages for four different drain voltages.

Another experiment comprised taking measurements during the preparation of a chip with microfluidics. The first measurement is done before wirebonding. The second measurement is done on the sample after wirebonding, prior to oxygen plasma etching in a barrel etcher. The time between these two measurements was a month. The third measurement is done immediately after oxygen plasma etching. Oxygen barrel etching is a standard treatment in IC technology to remove organic contaminants. The fourth measurement is done after the application of a polyester sealing layer, microfluidic cap, tubing, aluminum foil and with the chip clamped in the measurement box. The time difference between the second and fourth measurement was 2.5 hours. Two devices were measured simultaneously and the results are shown in Fig. 39. The threshold voltage and slope have been extracted and the values are listed in Table 4 and Table 5, respectively.

The results show that both devices show a similar change in threshold voltage and slope between phase 1 and 2. During phase 3 the threshold voltages do not change equally, and a larger difference arises in the saturation current between these devices. In phase 4 the devices shift with similar amounts in threshold voltage, but the difference in saturation current remains.

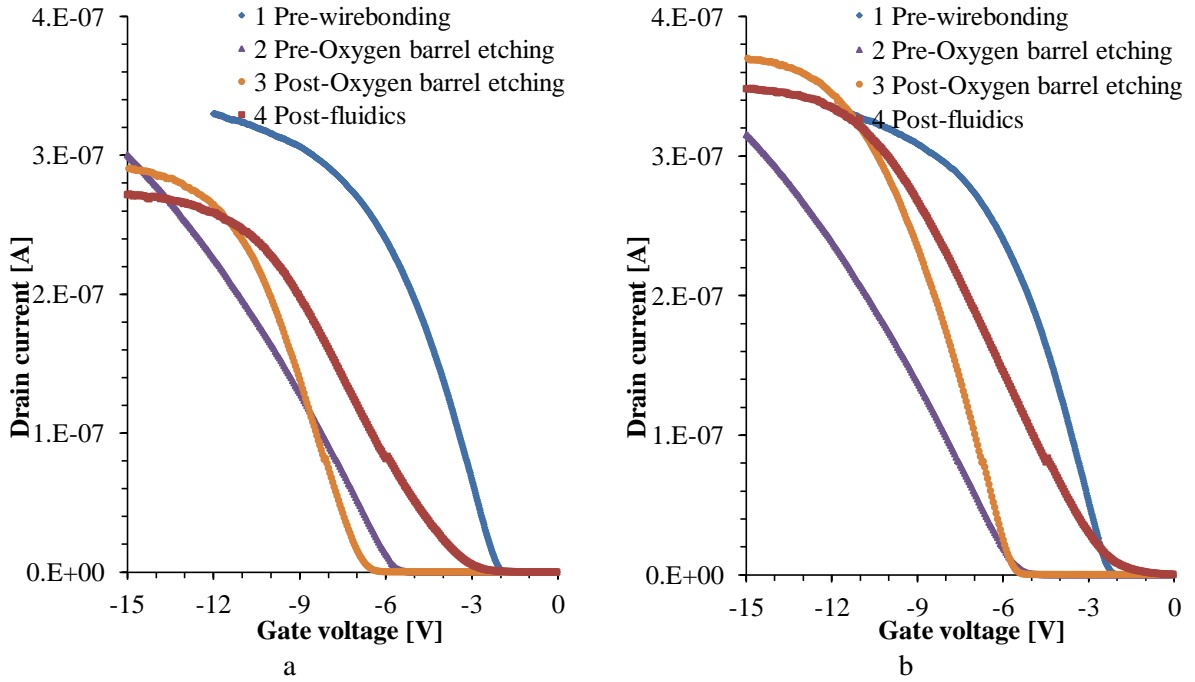


Fig. 39 Results from experiment on chip W2F3. Identical measurements were simultaneously performed on a) device 1 and b) device 2. I_D - V_G is measured at four points during preparations of a chip for measurements in liquid.

Phase	Device 1: V_{th1} [V]	ΔV_{th1} [V]	Device 2: V_{th2} [V]	ΔV_{th2} [V]	$V_{th1} - V_{th2}$ [V]
1	-2.22	-	-2.43	-	+0.21
2	-5.90	-3.68	-5.69	-3.26	-0.21
3	-6.85	-0.95	-5.74	-0.05	-1.11
4	-3.33	+3.51	-2.13	+3.62	-1.20

Table 4 Threshold voltage V_{th} for device 1 and 2 for different phases of preparation. The difference in threshold voltage is calculated between each phase and the one that follows it.

Phase	Device 1: minimum g_m [nA/V]	$g_m/g_{m,phase1}$	Device 2: minimum g_m [nA/V]	$g_m/g_{m,phase1}$	g_{m1}/g_{m2}
1	-82.10	1.00	-86.60	1.00	0.95
2	-42.65	0.52	-43.96	0.51	0.97
3	-69.26	0.84	-84.60	0.98	0.82
4	-41.77	0.51	-45.76	0.53	0.91

Table 5 Minimum g_m for device 1 and 2 for different phases of preparation.

6.1.1 Discussion

The nanowire sensors showed a remarkably high yield. Out of the 25 chips only one chip was rejected, because one device showed no characteristic. But based on observations in air, this could be because of a large negative shift that put the threshold voltage beyond the measured gate voltages.

The first experiment confirmed that the nanowire behaves as a linear resistor for small drain voltages. An interesting characteristic of the I_D - V_G curve of a nanowire is that the drain current levels off for higher negative gate voltages. It is hypothesized that the nanowire becomes fully accumulated with mobile charge carriers for higher negative gate voltages. In that situation a negative increase in gate voltage does not further increase the carrier density in the nanowire, resulting in the observed saturation. To explore this hypothesis, the nanowire device is first analyzed in its unbiased state.

With no bias applied to the nanowire at room temperature, the resistance of the contact leads and nanowire itself is determined by the dopant concentration and carrier mobility. The resistance can be calculated according to:

$$R = \frac{\rho L}{tW} \quad (9)$$

$$\rho = \frac{1}{qp\mu_p} \quad (10)$$

where R is the resistance, ρ is the resistivity, L is the length, W is the width, t is the thickness, q is the elementary charge ($1.6 \cdot 10^{-19}$ C), p is the hole carrier density, and μ_p is the mobility for holes. The resistivity of p-type silicon at room temperature doped with boron at a density of 10^{17} cm⁻³ is $2 \cdot 10^{-1}$ Ω·cm [23]. This low-doped part of the nanowire has a length of 3 μm, a width of 400 nm, and a thickness of 50 nm. This gives a resistance of 300 kΩ. The contact leads are doped at a density of 10^{19} cm⁻³ with a resistivity of $8.5 \cdot 10^{-3}$ Ω·cm [23]. The contact leads have a total length of 4 mm, a width of 100 μm, and a thickness of 50 nm. This ignores the tapered contacts and first and last 1 μm of the high-doped nanowire. This approximation gives a resistance of 68 kΩ. These results show that the nanowire has a higher resistance compared to the contact leads in a situation without voltage bias. The total series resistance is 368 kΩ. However, due to the relatively small ratio of nanowire resistance to contact lead resistance, the measurement's sensitivity to change in the resistance of the nanowire is less than optimal.

Next the resistances are calculated for a fully accumulated situation with an assumed hole concentration of 10^{21} cm⁻³ in both the nanowire and contact leads. Assuming the mobility stays constant, the resistance of the nanowire and contact leads is 30 and 680 Ω, respectively. The total series resistance is 710 Ω. With a drain-source voltage of 50 mV, this gives a current of $7 \cdot 10^{-5}$ A. There is a difference of two orders of magnitude when compared with the measured saturation current of approximately $3 \cdot 10^{-7}$ A. The measured resistance in saturation is approximately 167 kΩ.

An explanation for this discrepancy is that the biggest error likely lies with the component that undergoes the largest change. In this case that would be that nanowire, with four orders of magnitude. This would mean that both the contact leads and the nanowire will still decrease in resistance, but not as extremely as calculated. The physical cause behind this could be that the mobility decreases drastically as the induced amount of mobile charge carriers increases, negating the contribution of the increase in charge carriers to the conductivity. This would subsequently result in a saturation of the resistance as observed in the measurements.

It is expected that the nanowire is able to at least increase in carrier density to the same level as that of the contact leads (10^{19} cm⁻³), before the mobility is dominantly determined by carrier density. This would result in a nanowire resistance of 3 kΩ and a total series resistance of 71 kΩ, half of the measured value. Another way to approach this fully accumulated situation is to assume that the sheet resistance of the contact leads and the nanowire is equal, and then count the squares. The contact leads and nanowire consist of 40 and 7.5 squares, respectively. What both these methods show is that the ratio of the resistance of the nanowire to the contact leads decreases for stronger accumulation.

Returning to the application of measuring the dielectric constant, and reflecting on the impact of the above conclusions, another conclusion can be drawn. Firstly, the sensitivity in the zero bias situation is moderately good. Secondly, the dominating source of change in measured resistance originates from the nanowire in the zero bias and low accumulation region. This means that the dielectric constant can be measured by extracting the slope parameter from the IV-characteristic in this zero bias and low accumulation region. It is assumed that the currently used method already does this, by looking for and extracting the minimum slope. The presence of saturation limits the range of

this linear region and thus the area where the slope can be fitted for extraction. Nonetheless, these arguments combined suggest it is possible that the sensor is able to perform its intended purpose.

It is recommended that these sensors are redesigned to have a larger difference between the resistance of the nanowire and connection leads. This will improve the sensitivity in a two-point measurement and extend the region where the nanowire transconductance can be accurately measured. This can be done by decreasing the resistance of the connection leads and this in turn can be accomplished in two ways. The first method is to shorten the connection leads. But a consequence of this method is the shorter distance of the vias to the fluidic channel, increasing the risk of corrosion. The second method is to widen the connection leads. But this will come at the cost of extra space on the chip.

Another option does not involve changing resistances, but instead requires two extra connections to implement a four-point measurement. This allows one to isolate the resistance of the nanowire from the connection leads and therefore performs a more accurate measurement of the nanowire's resistance. This would also aid in the investigation into the cause responsible for the current saturation. To implement this method two more connection leads are required that connect as close as possible to the nanowire. This does cost space, but the advantage is that these connection leads can have a higher resistance and thus be narrow, as they are used to sense the voltage across the nanowire.

The properties of the nanowire sensors in air showed very similar characteristics in terms of transconductance, threshold voltage and saturation current in inter- and intra-die comparisons.

Measurements performed during the preparation of a chip showed that the extracted parameters of threshold voltage and transconductance can change during these necessary steps. The observed changes were always of equal sign, but could differ in magnitude. The results showed that during the oxygen plasma etching step such a difference in parameter values can be introduced.

The observed shifts in threshold voltage can be explained through changes affecting the magnitude of surface charge. However, the model of the nanowire sensor predicts the presence of two separate threshold voltages, associated with two separate transistors. One is associated with the top and sides of the nanowire sensor, and one associated with the bottom. As the bottom of the nanowire is not exposed to the environment, it is expected that this threshold voltage will be constant. Consequently its contribution to the total conduction is expected to be constant as well (see section 2.3). However, the results show a shift of the complete characteristic (see Fig. 39, phase 1 and phase 3). This implies that the threshold voltage associated with the bottom of the nanowire shifted in equal amount. However, it was just noted that this is not expected to happen. Based on these results it is hypothesized that instead of two separate transistors, the nanowire behaves like one transistor with surface charge influencing the threshold voltage. The control takes place through a combination of top and bottom coupling.

The theory cannot explain the observed differences in transconductance as observed in air. In practice however, the time between measurements and the number of measurements will influence the result. As is concluded in section 6.2 stabilization is required in order to compare results.

6.2 Properties in Water

This section discusses an experiment in which a new sample is exposed to demi-water for the first time. Comparisons are made between measurements in air and demi-water environments.

The experiment involves a sample with a polyester sealing, clamped in a measurement box and shielded from light. Measurements are repeated in cycles of five until all five consecutive I_D - V_G curves overlapped. First, this was done in air and subsequently in demi-water. Both measurements have been plotted in Fig. 40 for two devices on the same chip that were measured simultaneously. After obtaining a stable measurement in air, demi-water was introduced to the device surface.

Measurements were repeated with the same settings until a stable measurement was obtained. The threshold voltage and slope have been extracted from the first and last (stable) measurements and the values are listed in Table 6 and Table 7, respectively.

When comparing the two device characteristics in air, it is observed that both shift with the same amount during settling to a stable measurement. Their minimum slope does not change significantly during this process. When demi-water is introduced to the device surface, it is observed that the difference in threshold voltage between the two devices has decreased significantly and this remains true for the stable measurement. This effect has also been observed in experiments with other samples. The minimum slope in demi-water between the first and last measurement has decreased significantly. Remarkably, all changes in extracted parameters are identical in sign for both devices.

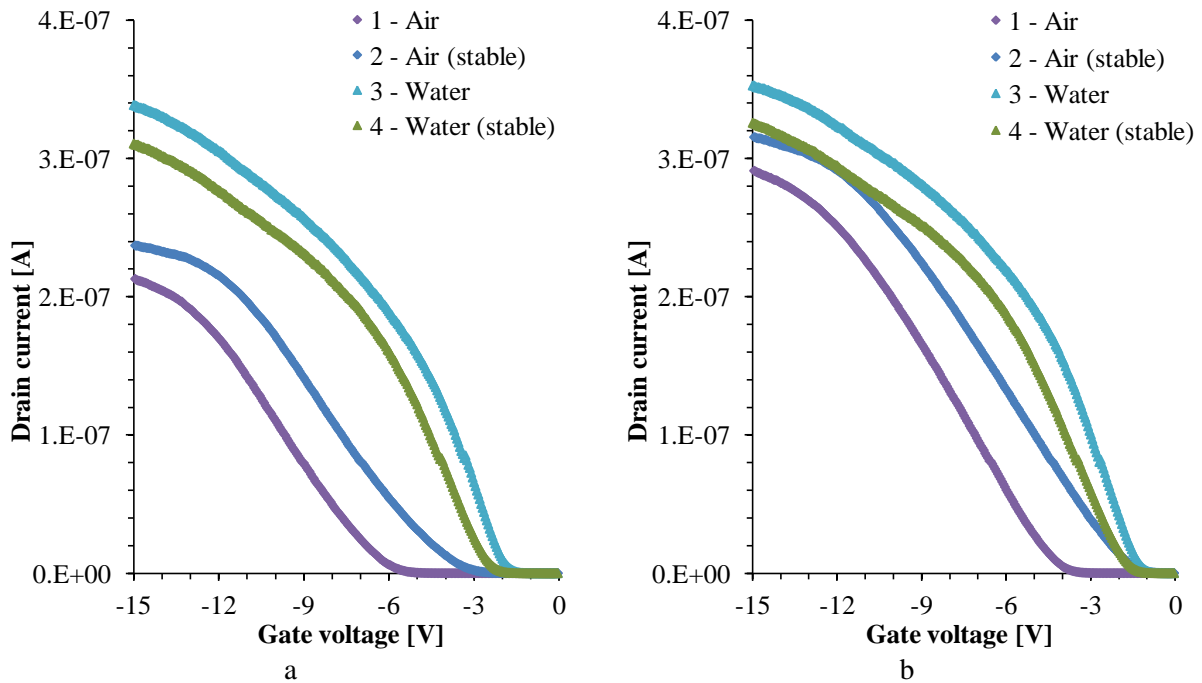


Fig. 40 Results from experiment on chip W2F3. Identical measurements were simultaneously performed on a) device 1 and b) device 2. I_D - V_G is measured in air and water. Both the first and last (stable) measurement in each environment is plotted.

Phase	Device 1: V_{th1} [V]	ΔV_{th1} [V]	Device 2: V_{th2} [V]	ΔV_{th2} [V]	$V_{th1} - V_{th2}$ [V]
1	-6.28	-	-4.30	-	- 1.98
2	-3.81	+2.47	-1.79	+2.51	-2.02
3	-1.99	+1.82	-1.37	+0.42	-0.62
4	-2.56	-0.57	-1.80	-0.43	-0.76

Table 6 Threshold voltage V_{th} for device 1 and 2 for different phases. The difference in threshold voltage is calculated between each phase and the one that follows it.

Phase	Device 1: minimum g_m [nA/V]	$g_m/g_{m,phase2}$	Device 2: minimum g_m [nA/V]	$g_m/g_{m,phase2}$	g_{m1}/g_{m2}
1	-34.95	1.05	-38.63	1.12	0.90
2	-33.14	1.00	-34.47	1.00	0.96
3	-65.70	1.98	-65.90	1.91	1.00
4	-53.13	1.60	-51.24	1.49	1.04

Table 7 Minimum g_m for device 1 and 2 for different phases.

6.2.1 Discussion

During the stabilization of measurements in air a large, equal, positive shift in threshold voltage was observed in both devices. Their slope showed only a small change. Upon introduction of demi-water, the threshold voltage difference between the two devices became smaller. This was observed in other experiments as well. The threshold voltage also became more positive. An important observation is that during the stabilization measurements the slope and threshold voltage change significantly. As a consequence, the extracted parameters from a first measurement are not reliable and stabilization is required in order to compare results.

6.3 Surface Modification

In this section experiments are described that involve switching between demi-water and dioxane on nanowire devices with a silicon oxide surface and a HMDS treated surface.

6.3.1 Silicon Oxide

The next experiment involved chip W2A5 with a polyester sealing. Two devices were measured in an identical manner and simultaneously. The results are shown in Fig. 41 and the extracted slope is listed in Table 8. The first measurement is in air, without previous exposure to liquids. There exists a significant difference in slope between the two devices. Their threshold voltage cannot be extracted. Next demi-water is introduced to the sensor surface. It is observed that the slope and threshold voltage of the two devices is now approximately equal. The threshold voltage of device 1 and 3 become -3.94V and -3.93V respectively. Next 1,4-dioxane is introduced to the sensor surface. The threshold voltage cannot be extracted. The slope of the two devices is again approximately equal, but has decreased significantly compared to the previous situation in water. When water is introduced again, device 1 returns to a similar threshold voltage (-3.81V) and slope compared with the first water measurement. The change in threshold voltage and slope belonging to device 2 show a similar trend, but do not occur with the same magnitude. Again switching to 1,4-dioxane shows that the slope parameter for both devices are similar to each other and to the previous measurement in dioxane. It is

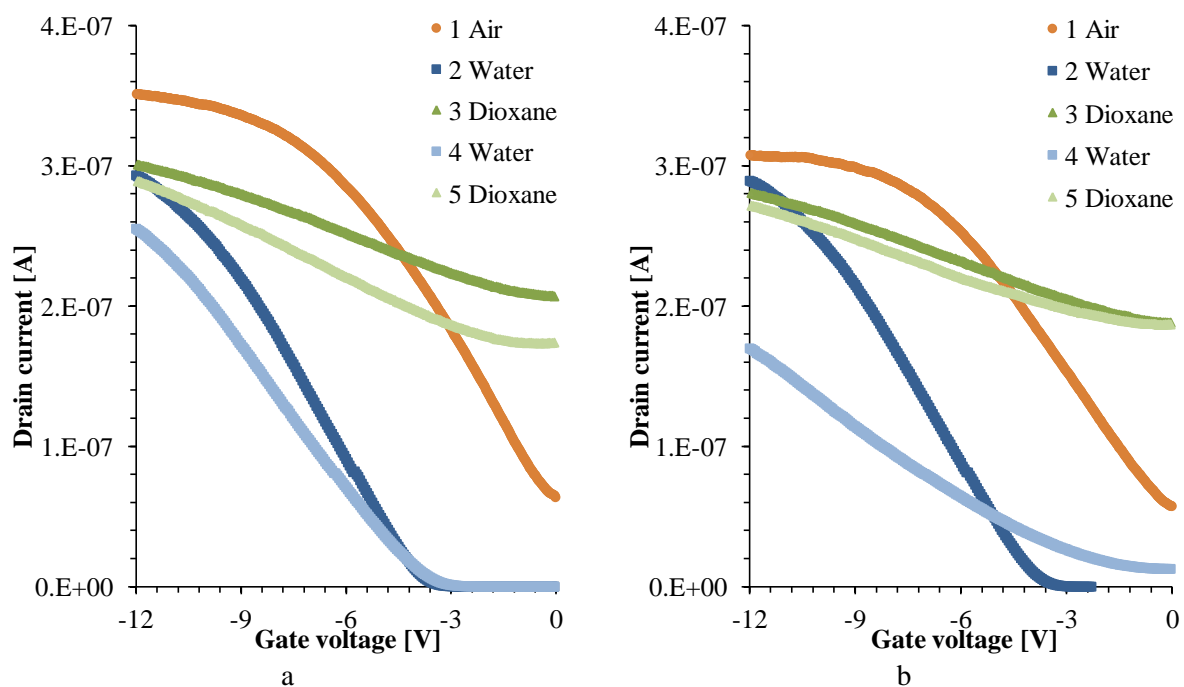


Fig. 41 Results from chip W2A5. Identical measurements were simultaneously performed on a) device 1 and b) device 3. I_D - V_G is measured in air, water and dioxane.

noted that there is only a single period of flow at the beginning of each phase to introduce the new liquid. During the subsequent measurements, the pump is turned off and there is no flow. Pump time, time to plotted measurement, total time of liquid on the sensor surface, and the total number of measurements are listed in Table 9 for each phase.

Obtaining a stable measurement takes a certain amount of time, or a number of measurements, or a combination thereof. As shown in Fig. 42 there is a gradual shift in the I_D - V_G characteristic when the dioxane on the sensor surface has been replaced with demi-water. Here it is observed that the amount of shift decreases with each next measurement. Also observed in Fig. 42 is that the measurements for phase 4 of device 3 show an initial sudden decrease in saturation current. However, this observation is of a non-reproducible condition.

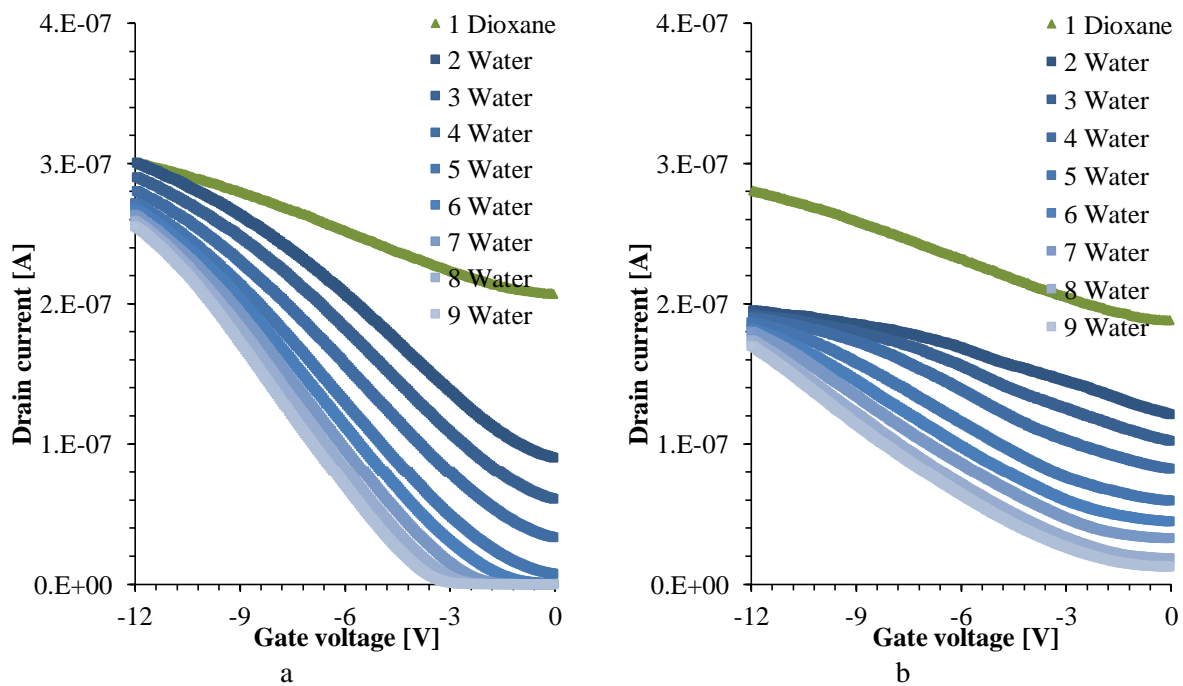


Fig. 42 Detail of the results from chip W2A5. Identical measurements were simultaneously performed on a) device 1 and b) device 3. These plots show the settling behavior with intermediate measurements when switching from phase 3 to phase 4 as shown in Fig. 41.

Phase	Device 1: minimum g_m [nA/V]	$g_m/g_{m,phase2}$	Device 3: minimum g_m [nA/V]	$g_m/g_{m,phase2}$	g_{m1}/g_{m2}
1	-51.94	1.11	-41.55	0.91	1.25
2	-46.68	1.00	-45.77	1.00	1.02
3	-11.83	0.25	-11.53	0.25	1.03
4	-37.29	0.80	-21.42	0.47	1.74
5	-14.85	0.32	-11.32	0.25	1.31

Table 8 Minimum g_m for device 1 and 3 for different phases of liquid environment.

Phase	Pump time [min]	Time to measurement [min]	Total time [min]	# of measurements
1	-	-	-	-
2	15	29	120	2
3	29	60	71	4
4	29	105	114	8
5	25	48	58	3

Table 9 The pump time used to introduce the new liquid, the time the liquid was on the surface until the measurement (incl. pump time), the total time of a liquid on the sensor surface, and the total number of measurements that were executed are listed.

The next experiment involved chip W2F7 with a polyester sealing. One device was measured. The results are shown in Fig. 43 and the extracted slope is listed in Table 10. Timing and measurement data are listed in Table 11. The first measurement is in demi-water without previous exposure to any liquid. Next dioxane is introduced and measurements are performed, and finally measurements are performed again in demi-water. The measurements are not stabilized.

It is observed that the threshold voltage associated with the first measurement in water is positive (1.86V). The threshold voltages of the subsequent measurements in dioxane and water cannot be determined. They cannot be estimated either, because it is known that during settling and stabilization of the measurement the threshold voltage can change significantly, as seen in Fig. 42. The same holds for the measurement in water, where it is observed that the measurement has not yet stabilized. This threshold voltage is shifting and becoming less positive (data not shown). It is observed that the saturation current decreases significantly in an environment of dioxane and returns to the previous level in water.

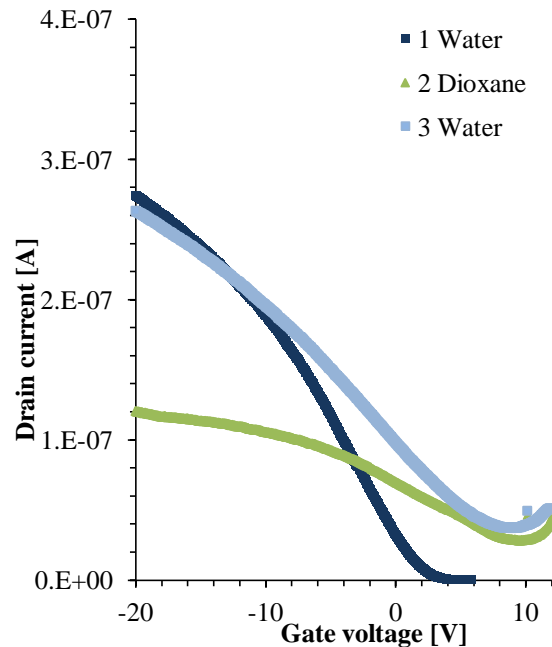


Fig. 43 Results from chip W2F7. I_D-V_G is measured of device 2 in water and dioxane.

Phase	Device 2: minimum g_m [nA/V]	$g_m/g_{m,phase1}$			
1	-20.10	1.00			
2	-7.75	0.39			
3	-12.77	0.64			

Table 10 Minimum g_m for device 2 for different liquid environments.

Phase	Pump time [min]	Time to measurement [min]	Total time [min]	# of measurements	
1	12	36	49	3	
2	12	19	55	1	
3	7	14	30	1	

Table 11 The pump time used to introduce the new liquid, the time the liquid was on the surface until the measurement (incl. pump time), the total time of a liquid on the sensor surface, and the total number of measurements that were executed are listed.

The next results come from the continuation of the experiment described in section 6.2. Those results were from air and upon the first introduction of water to the device surface. The stable measurement in water forms the starting point of the following results.

These results (see Fig. 44a-b) were all preceded by a pumping time of 10 minutes. Measurements were then repeated until the measured characteristic had stabilized. The timing data and measurement numbers are listed in Table 14. The threshold voltage and slope have been extracted and the values are listed in Table 12 and Table 13, respectively.

It is observed from the measurement in dioxane that the saturation current has decreased for both devices compared to water. However, the smaller slope is remarkable, which is approximately constant over a larger range of gate voltages compared to the measurements in air and water. With the reintroduction of water, the threshold voltage shifts to negative values again, even exceeding that of the first measurement in water. It is further observed that the difference in threshold voltage between the two devices remains constant compared to the first measurement in water. Interestingly, the slope of both devices is approximately equal again to the value of the slope in the first measurement in water.

In terms of timing, the pumping time of each liquid has been kept constant. The total time the liquid was kept on the sensor surface was dependent on the amount of measurements necessary to obtain a stable measurement. Despite the time listed for the first water measurement, it actually only required 30 minutes in total to obtain a stable measurement. But the water remained on the sensor for an even longer period until eventually dioxane was pumped in. It is observed that stabilizing the first measurements in water required fewer measurements and thus less time as compared to dioxane and water from phase 2 and 3, respectively. Stabilization in dioxane and subsequently in water took longer, and approximately equal amounts of time and measurements.

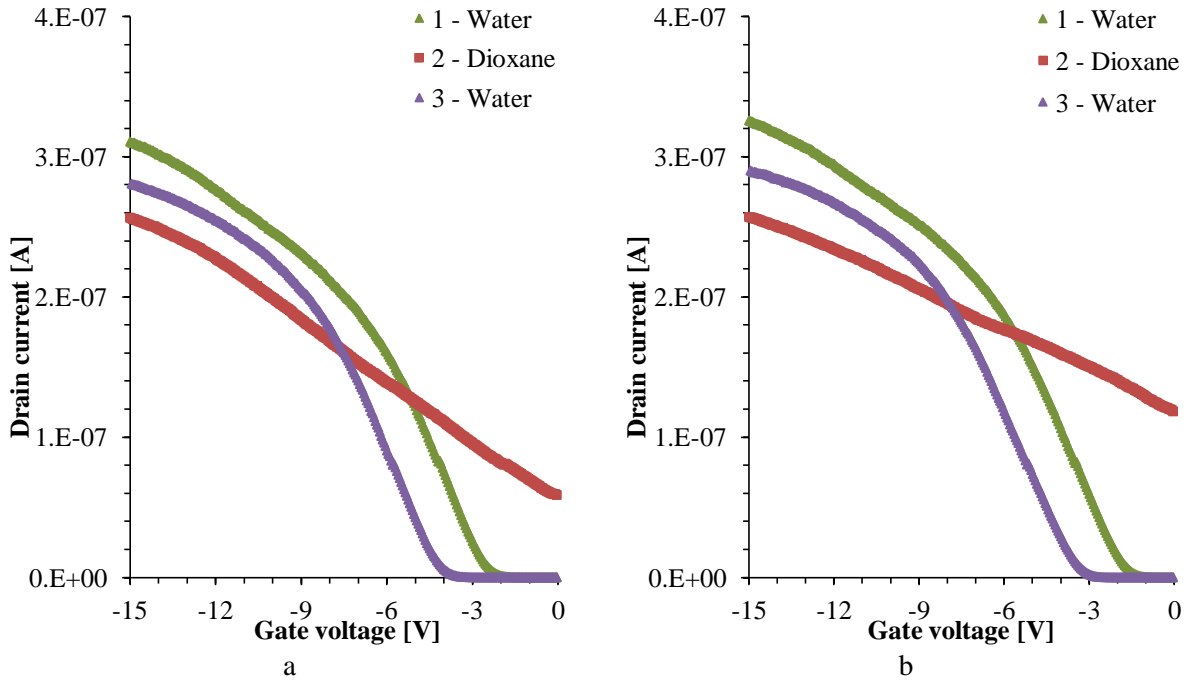


Fig. 44 Results from chip W2F3 for a) device 1 and b) device 2. Plotted are the I_D - V_G characteristics for three successive phases (water, dioxane, and water).

Phase	Device 1: V_{th1} [V]	ΔV_{th1} [V]	Device 2: V_{th2} [V]	ΔV_{th2} [V]	$V_{th1} - V_{th2}$ [V]
1	-2.56	-	-1.80	-	-0.76
2	-	-	-	-	-
3	-4.17	-	-3.44	-	-0.73

Table 12 Threshold voltage V_{th} for device 1 and 2 for different phases. The difference in threshold voltage is calculated between each phase and the one that follows it.

Phase	Device 1: minimum g_m [nA/V]	$g_m/g_{m,phase1}$	Device 2: minimum g_m [nA/V]	$g_m/g_{m,phase1}$	g_{m1}/g_{m2}
1	-53.13	1.00	-51.24	1.00	1.04
2	-18.15	0.34	-14.49	0.28	1.25
3	-53.86	1.01	-50.40	0.98	1.07

Table 13 Minimum g_m for device 1 and 2 for different liquid environments.

Phase	Pump time [min]	Time to measurement [min]	Total time [min]	# of measurements
1	10	31	55	5
2	10	62	67	12
3	10	66	163	13

Table 14 The pump time used to introduce the new liquid, the time the liquid was on the surface until the measurement (incl. pump time), the total time of a liquid on the sensor surface, and the total number of measurements that were executed are listed.

6.3.2 Discussion

In the first experiment it is observed that the introduction of water results in both devices having a similar threshold voltage and minimum slope value. It is thought that the reason behind this apparent equalization is due to the introduction of a liquid. The liquid environment, as opposed to air, allows

for the entire surface to reach an equal surface condition. It is also observed that the minimum slope for dioxane is lower compared to the slope in water. This is in agreement with theory.

Another observation is related to the stabilization of a measurement. It is observed that a certain amount of time, or a number of measurements, or a combination thereof is required to obtain a stable measurement. A clear example of this is shown with the stabilization in water. It is shown that after pumping water, each consecutive measurement shows a shift to more negative values for the threshold voltage. The behavior of this shift is compared to the charging of a capacitor through a resistor, characterized by its RC time constant. This is because the amount of shift was observed to be initially large, but decreasing with each next measurement. This shows that extraction of the threshold voltage and minimum slope from the first measurement cannot be recommended. Instead the characteristic should first be stabilized.

The second experiment showed a significant, but reversible decrease in the saturation current for dioxane, compared to water. Upon reintroduction of water, the characteristic appears similar again to the previous measurement in water. However, these measurements were not stabilized and of a non-reproducible condition.

In the third experiment it is observed that the slope as measured in water, before and after a dioxane step, is approximately equal. Also this experiment again confirms that the slope of dioxane is measured to be lower than that for water. This is in accordance with the theory (see section 2.4.1).

It takes longer to obtain a stable measurement in dioxane and also with water afterwards. One possible reason is that the previous liquid did not get pumped out of the sensor microfluidics completely. After pumping is stopped, the previous liquid that remains mixes with the bulk of the new liquid, requiring a longer time to stabilize. This aspect can be thought of as a part of a larger concept. In this concept there are three dominant time constants that determine how long it takes before a stable measurement can be made. The first time constant is to do with replacing the bulk of the liquid in the sensor microfluidics. The second time constant is the process where the liquid around the sensor and nearer the interface is in equilibrium with the bulk, dominated by diffusion. The third time constant is related to the number of measurement cycles required to stabilize the interface. With this concept in mind, it will take longer for measurements to stabilize when a previous liquid was present. This is because the mixing will increase the time it takes for equilibrium to establish.

Another observation is a trend with the stabilization in a water environment. During settling to a stable measurement the threshold voltage always shifts to more negative values, as shown for example in Fig. 42. This again shows the importance of stabilization.

6.3.3 Evaporation of Dioxane

The experiment that is discussed above was continued, switching between water and dioxane two more times. But these measurements ran into a practical problem concerning the evaporation of dioxane from the tubing. Approximately 22 minutes after pumping had stopped a very abrupt change occurred in the measured characteristic. The same observation is made for the third time that dioxane was pumped in and measured, this time approximately 23 minutes after pumping had stopped. When dioxane was measured for the third time it was observed that the dioxane had evaporated from the outlet tubing exactly before the measurement was performed in which the abrupt change is observed.

The correlation in time between the observable evaporation of dioxane from the tubing and the abrupt change in the measured characteristic raises doubt whether there is still dioxane on the sensor surface. It is also noted that the characteristic after the abrupt change is similar to that of a typical result in water or air (see Fig. 45). Based on these two arguments it seems likely that these measurements (after the abrupt change) in 'dioxane' were not performed in a purely dioxane environment. Unfortunately, the measurements before the abrupt change cannot be used as they had not stabilized. Another observation is that the saturation current decreases for each successive phase,

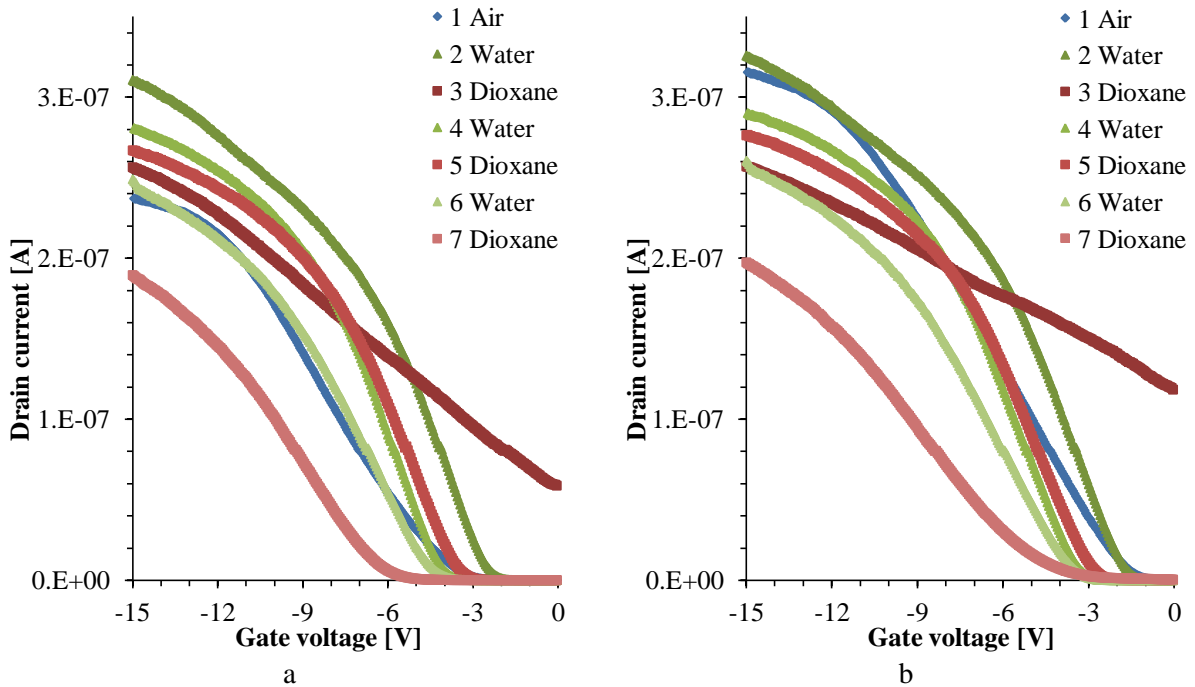


Fig. 45 Plot of a) device 1 and b) device 2 of chip W2F3. It shows the stable measurements of the complete experiment.

when the air (phase 1) and first dioxane (phase 3) measurements are ignored.

6.3.4 HMDS Surface

As explained in section 5.2.2 it is expected that the pK_a of the silanol groups will increase when exposed to dioxane. One way to stabilize this interface is to treat it with hexamethyldisilazane (HMDS). This treatment will terminate the silicon oxide with trimethylsilyl groups ($-\text{Si}(\text{CH}_3)_3$), which are chemically less reactive compared to silanol groups ($-\text{OH}$). This process is illustrated in Fig. 46. Diminishing the variation in surface charge as caused by the interface allows for a better observation of the effects when changing the dielectric constant.

The first step in treating a silicon oxide surface with HMDS is with an oxygen plasma etching step. This is performed in a barrel etcher. The device, wirebonded in a chip carrier, is placed inside a metal meshed-barrel in the etcher. The barrel will act as a faraday cage and prevent the sample from being damaged with the ions produced by the plasma. In this low pressure environment the oxygen radicals can travel towards the sensor surface and will react with any organic contaminants on the surface and remove them as volatile products are formed as a result. With the surface now cleaned the device is ready to be treated in another machine with gaseous HMDS. Before exposure to HMDS the chip is heated to $150\text{ }^\circ\text{C}$ and several purges with gaseous N_2 take place to remove water from the chip surface. The purpose of all these preparatory steps is to ensure a good coverage.

To verify the effectiveness of the treatment a bare silicon wafer with silicon oxide was used as a sample and treated with HMDS. The contact angle was measured as shown in Fig. 47 with a drop of demi-water and was found to be $70\text{-}75^\circ$ both before and after 17 hours of exposure to liquid 1,4-dioxane. It is noted that the contact angle, and thus the coverage, could be further increased up to $110\text{-}120^\circ$ by increasing the process temperature. It was observed that the contact angle of the untreated wafer was small and can be classed as hydrophilic. It was further observed that 1,4-dioxane on the HMDS-treated wafer spread out immediately on contact resulting in a similarly small contact angle.

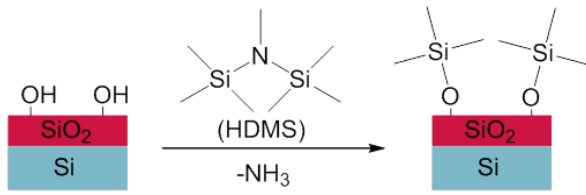


Fig. 46 A silicon oxide surface with silanol groups (left) is treated with gaseous HMDS (middle) resulting in a surface termination with trimethylsilyl groups.

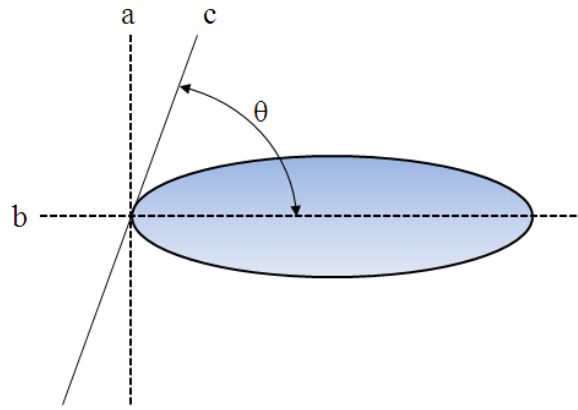


Fig. 47 schematic illustration of a contact angle (70° shown) measurement. Line *b* is aligned with the mirror plane of the droplet on the substrate. Line *a* is then aligned with the end of the droplet. Line *c* can rotate on the crossing point of line *a* and *b* and is aligned with the gas-liquid interface. The resulting angle θ between plane *c* and *b* as measured through the liquid is the contact angle.

The next experiment was performed to study the influence of oxygen plasma etching and the HMDS treatment on the gate current. Ideally, the substrate is isolated from the nanowire sensors by the 300 nm silicon oxide BOX layer. However, a small current is measured. In this experiment two chips are compared. Both chips are treated with an oxygen plasma etching step in a barrel etcher, but only one is treated with gaseous HMDS afterwards. After each step measurements are performed to track the effect on the gate current.

The measurements are performed with the gate voltage swepted in a continuous mode. For both

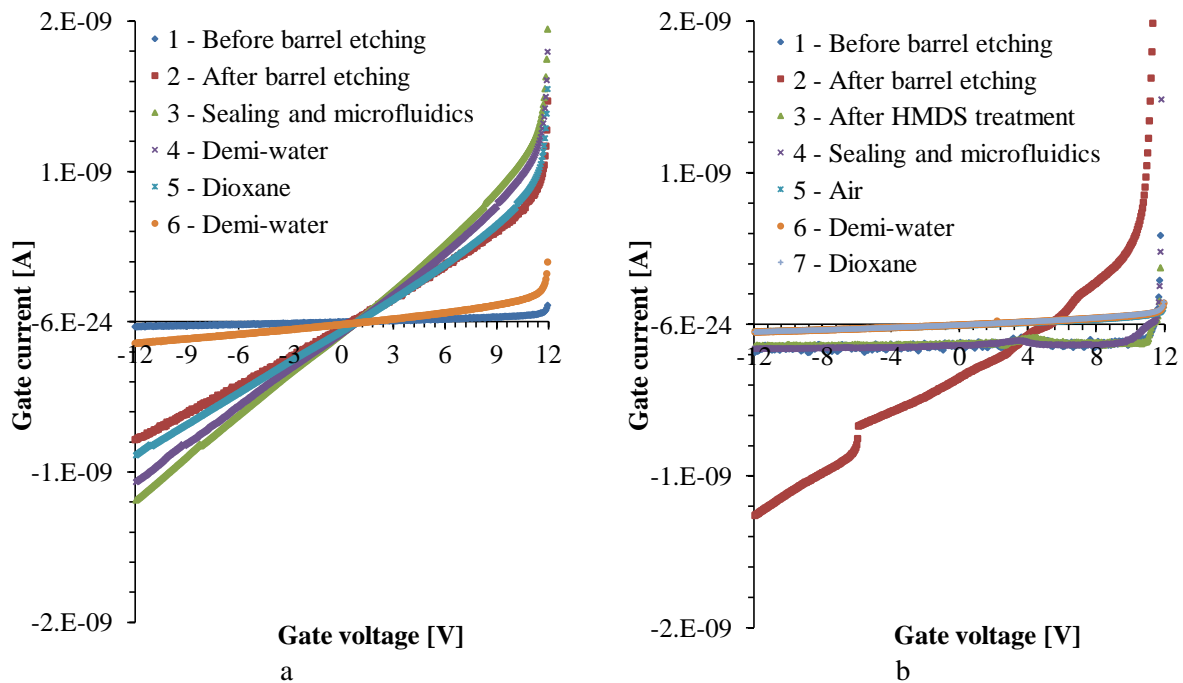


Fig. 48 Plots of gate current versus gate voltage for two separate chips. a) chip W2F7 without HMDS treatment. The gate current shows a large increase after the barrel etching step. The demi-water at step 6 is measured 19 hours after step 5 and shows the gate current has decreased significantly b) chip W2F9 with HMDS treatment. The gate current shows a large increase after the barrel etching step as well, but returns to the previous level immediately after HMDS treatment. The elapsed time between step 4 and 5 is 17 hours.

chips two of the three devices had a drain voltage of 50 mV, and one biased at 5 mV. The results are shown in Fig. 48 and Fig. 49. It is observed that for both chips the gate current increases significantly after the oxygen plasma etching. For the chip that is subsequently treated with HMDS the gate current decreases to approximately the same level it was before the etching step and remains this way also in a liquid environment. The gate current on the chip without the HMDS treatment stayed at the increased level. Interestingly, the gate current decreased significantly after the chip without HMDS treatment had spent 19 hours in demi-water.

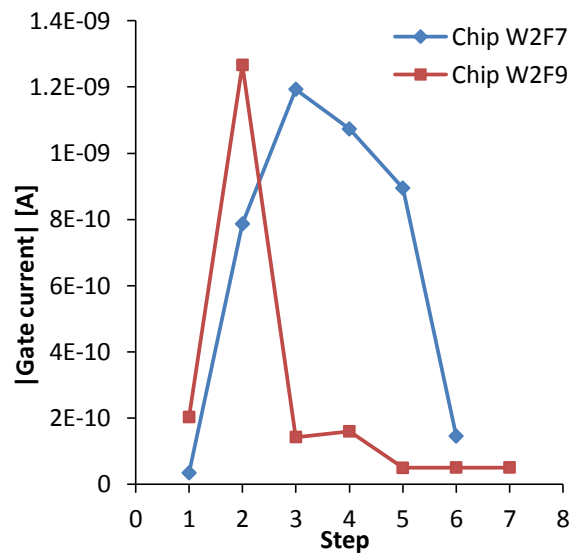


Fig. 49 Gate current of chip W2F7 (without HMDS) and W2F9 as measured after each step (see Fig. 48 for details) for $V_G = -12$ V.

The next experiment discusses the results of chip W2D9 that has been treated with HMDS. A mixture of 50% water and 50% dioxane (by volume) is alternated with demi-water as the fluid on the chip's surface. The results in Fig. 50a were obtained with a pump time of 5 minutes, followed by a measurement and then the next pumping step. These measurements were not stabilized. The results in Fig. 50b were obtained with an identical method but with a pumping time of 20-35 minutes between measurements.

Comparing the two series of measurements, it is observed that the threshold voltage is significantly more negative after longer pumping times.

Furthermore, it is observed that the measured drain currents are significantly lower compared to those of nanowires from other experiments. It is noted that the experiment was performed with a chip which had already been extensively used. However, earlier measurements of the same nanowires show current levels that did reach typical values. But this maximum current gradually decreased during the experiments that followed.

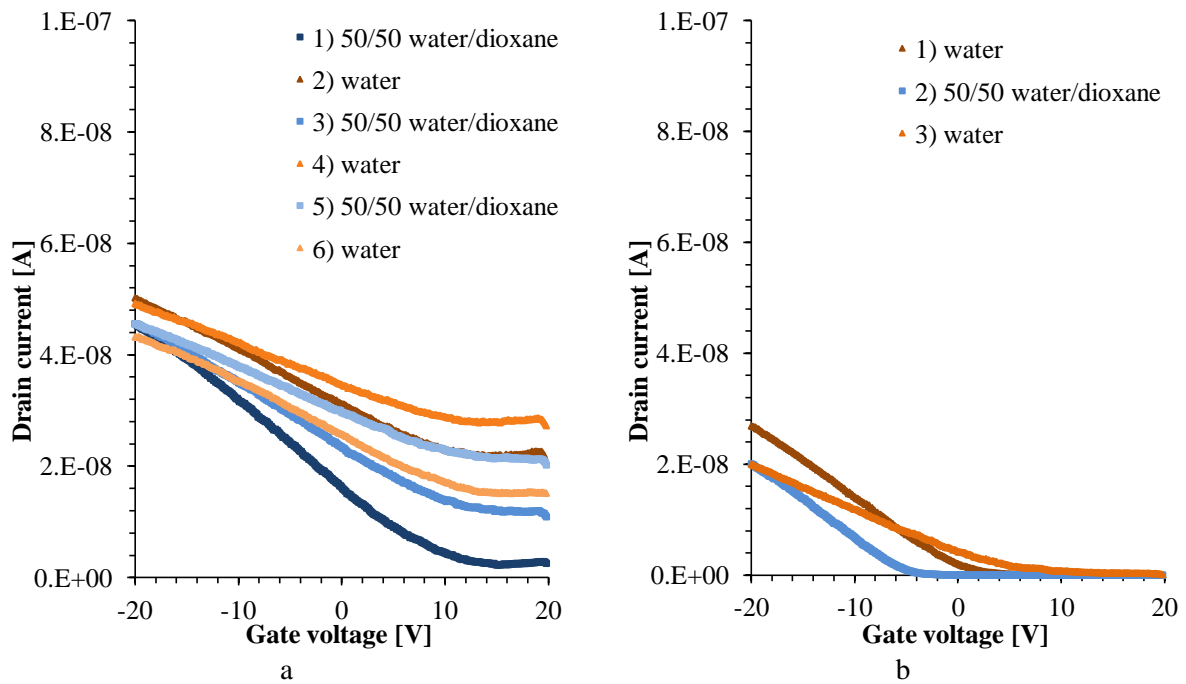


Fig. 50 Plot of I_D - V_G characteristics for device 2 for two experiments: a) pumping for 5 minutes, performing a measurement, and pumping the next liquid, b) similarly but pumping for 20-35 minutes.

6.3.5 Discussion

The silicon oxide surface of a nanowire sensor was successfully modified with HMDS in order to decrease variation in surface charge. Furthermore, it was shown that this new surface is compatible with 1,4-dioxane and is not damaged by it.

The second experiment investigated the influence of oxygen plasma etching and a HMDS treatment on the gate current. The gate current is likely due to leakage along the surface of the chip. It is expected that the BOX layer is isolating, but in this situation the thin oxide on the nanowire sensors can lead to a tunneling current from the drain and source to the gate. It is observed that the gate current increases with both chips after the oxygen plasma etching step. This is likely due to the clean SiO_2 surface terminated with OH-groups. Upon contact with air a thin water film will form on the hydrophilic surface and increase the leakage. As the results confirm, a subsequent HMDS treatment terminates the silicon oxide with a hydrophobic surface and this suppresses the leakage along the surface. Without such a treatment the surface remains at an increased level of conduction. But it is observed that with time these untreated surfaces also arrive at a state where the leakage current has returned to the pre-plasma level.

Furthermore, it was observed that the time spent pumping a new liquid onto the chip has a large effect on the measured threshold voltage. This is in agreement with the previous findings that concluded that time is an important factor in obtaining a stable and reliable measurement. A longer pumping time better replaces the liquid on the chip and the longer time allows for more settling to take place of surface conditions.

It was also observed in the last experiment that the current passing through the nanowire appears to degrade with time and measurements. However, due to the limitations of a two-point measurement, it is difficult to identify a cause as one cannot distinguish between the contribution in resistance from the nanowire and the contact leads. It is recommended to implement a four-point measurement in order to further investigate this phenomenon.

7 Conclusion

A reliable measurement setup has been established to characterize nanowire sensors in various environments. In combination with this setup a measurement protocol has been developed which defines measurement programs and their settings. Possible error sources have been identified and solutions have been implemented. The measurement artifacts originating from the Keithley measurement system were of particular importance. Based on the theory of the nanowire field-effect sensor two relevant parameters have been identified for measuring the dielectric constant of liquids: the threshold voltage, and transconductance. A method has been developed successfully in order to extract these parameters from the measurement data.

Dioxane has been selected as the liquid to complement water for characterization of the nanowire sensor, due to its low dielectric constant and miscibility. However, dioxane is a strong organic solvent and was found to cause leakage in the old microfluidic setup. The microfluidic system has been analyzed and its weak points have been identified. As a result several solutions have been investigated. Finding a suitable material for the sealing layer proved to be of particular importance and difficulty. It was found that a sealing layer based on an acrylic adhesive on a polyester carrier proved sufficiently durable. In addition, silicone rubber has been identified as a suitable tubing material. These efforts resulted in a microfluidic setup that successfully contained the liquids for the duration of the experiments as reported in this research.

The nanowire sensors showed a remarkably high yield. Their properties in air showed very similar characteristics in terms of transconductance, threshold voltage and saturation current in inter- and intra-die comparisons. The first experiments in air confirmed that the nanowire behaves as a linear resistor for small drain voltages, in agreement with theory. An interesting characteristic of the I_D - V_G curve of a nanowire is that the drain current levels off for higher negative gate voltages, referred to as current saturation.

Calculations helped identify the possible cause of the saturation. These calculations also show that the sensor is able to perform its intended purpose based on the following arguments. Firstly, the sensitivity in the zero bias situation is moderately good. Secondly, the dominating source of change in measured resistance originates from the nanowire in the zero bias and low accumulation region. This means that the dielectric constant can be measured by extracting the slope parameter from the IV-characteristic in this zero bias and low accumulation region. It is further assumed that the currently used method already does this, by looking for and extracting the minimum slope. The presence of saturation limits the range of this linear region and thus the area where the slope can be fitted for extraction.

Based on these conclusions it was recommended that these sensors are redesigned to have a larger difference between the resistance of the nanowire and connection leads and solutions were described. This will improve the sensitivity in a two-point measurement and extend the region where the nanowire transconductance can be accurately measured. Another option that was described does not involve changing resistances, but instead requires two extra connections to implement a four-point measurement. This allows one to isolate the resistance of the nanowire from the connection leads and thus perform a more accurate measurement of the nanowire's resistance. This would also aid in the investigation into the cause responsible for the current saturation.

Measurements performed during the preparation of a chip showed that the extracted parameters of threshold voltage and transconductance can change during these necessary steps. The observed changes were always of equal sign, but could differ in magnitude. The observed shifts in threshold voltage can be explained through changes affecting the magnitude of surface charge. The model of the

nanowire sensor predicts the presence of two separate threshold voltages, associated with two separate transistors. This is however not observed in the measurements. Based on these results it was hypothesized that instead of two separate transistors, the nanowire behaves like one transistor with surface charge influencing the threshold voltage. The control takes place through a combination of top and bottom coupling.

The next results focused on stabilization in air and water. During the stabilization of measurements in air a large, positive shift in threshold voltage was observed. Furthermore, the slope showed only a small change. Upon introduction of demi-water, it was observed that the threshold voltage became more positive. During stabilization, the threshold voltage always shifts to more negative values. It was further observed that the difference in slope and threshold voltage between devices became smaller. It is hypothesized that the liquid environment equalizes the surface condition across the surface of the chip. An important observation is that during the stabilization measurements in both air and water the slope and threshold voltage change significantly. As a consequence, the extracted parameters from the first measurement are not reliable and stabilization is required in order to compare results.

Experiments that compared water with dioxane showed that dioxane results in a smaller minimum slope compared to the slope in water. This is in agreement with theory which predicts that the lower dielectric constant of dioxane will result in a weaker coupling of the electric field through the liquid. Furthermore, these changes were reversible when measuring the properties in water again or in dioxane.

Another important observation was made related to the stabilization of a measurement in water and dioxane. It was observed that a certain amount of time, or a number of measurements, or a combination thereof is required to obtain a stable measurement. This behavior was compared to the charging of a capacitor through a resistor, characterized by its RC time constant. This again showed that extraction of the threshold voltage and minimum slope from the first measurement cannot be recommended. Instead the characteristic should first be stabilized.

It was also observed that it takes longer to obtain a stable measurement in a liquid when a different liquid had preceded it. Based on these results it was hypothesized that there are three dominant time constants that determine how long it takes before a stable measurement can be made. The first time constant is to do with replacing the bulk of the liquid in the sensor microfluidics. The second time constant is related to the process where the liquid around the sensor and nearer the interface moves toward equilibrium with the bulk, dominated by diffusion. The third time constant is related to the number of measurement cycles required to stabilize the interface. According to this theory it will take longer for measurements to stabilize when a previous liquid was present, because the mixing will increase the time it takes for equilibrium to establish.

The silicon oxide surface of a nanowire sensor was successfully modified with HMDS in order to decrease variation in surface charge. Furthermore, it was shown that this new surface is compatible with 1,4-dioxane and is not damaged by it.

Another experiment investigated the influence of oxygen plasma etching and a HMDS treatment on the gate current. The gate current is likely due to leakage along the surface of the chip. It is expected that the BOX layer is isolating, but in this situation the thin oxide on the nanowire sensors can lead to a tunneling current from the drain and source to the gate. It is observed that the gate current increases with both chips after the oxygen plasma etching step. This is likely due to the clean SiO₂ surface terminated with OH-groups. Upon contact with air a thin water film will form on the hydrophilic surface and increase the leakage. As the results confirm, a subsequent HMDS treatment terminates the silicon oxide with a hydrophobic surface and this suppresses the leakage along the

surface. Without such a treatment the surface remains at an increased level of conduction. But it is observed that with time these untreated surfaces also arrive at a state where the leakage current has returned to the pre-plasma level.

Furthermore, it was observed that the time spent pumping a new liquid onto the chip has a large effect on the measured threshold voltage. This is in agreement with the previous findings that concluded that time is an important factor in obtaining a stable and reliable measurement. A longer pumping time better replaces the liquid on the chip and the longer time also allows for more settling to take place of surface conditions.

It was also observed that the current passing through a nanowire appears to degrade with time and measurements. However, due to the limitations of a two-point measurement, it is difficult to identify a cause as one cannot distinguish between the contribution in resistance from the nanowire and the contact leads. It is recommended to implement a four-point measurement in order to further investigate this phenomenon.

In summary, the main conclusions are the following. Based on calculations and experimental evidence the nanowire sensor has been shown to work and a change in transconductance of the sensor was successfully measured between water and dioxane. Recommendations were made to improve the sensitivity and accuracy of these measurements. Important conclusions were also made relating to the measurement methodology. The first conclusion is that just one measurement is not reliable and stabilization is required. The second conclusion is that time and the number of measurements are important parameters in this stabilization process. And finally, for each specific system these parameters could behave differently, requiring the identification of the dominant parameter in order to develop a reliable measurement protocol.

8 Recommendations

This chapter lists recommendations divided into three aspects of the research: experiments, measurement setup, and device design. The first section proposes new experiments that would be key to further our understanding on how to measure the dielectric constant of liquids. The second and third section discuss improvements to respectively the measurement setup and device design.

8.1 Experiments

- In section 5.2.1 an observation is made of residue on the chip surface. It is recommended to perform an analysis of this residue in order to determine its cause.
- In section 6.3.3 the problem of evaporation of dioxane from the setup is described. Two methods are proposed in order to keep dioxane in the setup and on the chip's surface. The first method is based on the observation that silicone tubing is highly permeable to dioxane and so a solution involves finding a less permeable tubing type. The second proposed method is to keep the pump on and maintain flow.
- In section 6.3.4 the surface treatment with HMDS is described. An advantage of this treatment is that it is assumed to reduce variation in surface charge when different liquid mixtures are introduced to the sensor. This will allow better observation of the effect of the dielectric constant upon the device characteristic. The treatment of the sensor surface with HMDS and its compatibility with dioxane has been shown to be successful, but no stabilized measurements have yet been performed. Validation with stabilized measurements will show if the HMDS treatment works as intended. This could then be followed up by measuring for different mixtures of water and dioxane, in order to further investigate the sensing mechanism.
- Finally, the theory described in chapter 2 models the liquid environment as an insulating material with a certain dielectric constant. It would be interesting to investigate how the current model could be improved to account for the presence of ions in a liquid.

8.2 Measurement Setup

- In section 4.3.2 it is described that handling has an influence on the measured characteristic. Currently, when a new liquid is pumped across the chip, the tubing has to be changed and handled. One way to avoid handling is to use a Y-shaped coupler. This would let the flow from the two syringes merge into the tubing leading to the chip. Changing between the liquids can then be accomplished by turning on and off the appropriate pumps.
- Section 5.5 describes a problem when trying to create a leaktight seal between the microfluidic cap and chip surface. When using non-sticky sealing layers it was observed that leakage often occurred towards the far end of the clamp. This is likely because the clamping force was not applied equally across the cap surface. This is an inherent problem when using a lever-type clamp. In case future experiments require the use of non-sticky sealing layers, it is recommended to use a two or four point clamping system to apply an equal clamping force across the cap to improve the sealing.
- Related to the same problem, it is further suspected that the small borders around the channel in the microfluidic cap are not wide enough to allow for a good seal. A redesign of the microfluidic cap should take this into account.

8.3 Device Design

- Corrosion of the aluminum connections has been observed where it comes into contact with the solution (see section 5.2.3). Coating these aluminum connections with a protective layer could prevent this from occurring. This would also allow for the vias to be closer to the fluidic channel and in turn allow for shorter silicon contact leads. This will help with improving the ratio of the resistance of the nanowire to the contact leads, as is essential in a two-point measurement.
- The sensitivity to change in the dielectric constant of the liquid can be further improved by optimizing the device shape. This can be done by maximizing the capacitive coupling through the liquid relative to the coupling only through the underlying dielectric. This will likely result in a fin-like shape.
- It has been suggested that a nanowire device could be coated in post-processing and then serve as a reference device during experiments. A better idea might be to create this reference device already during fabrication (see section 3.2). This could be done by not opening up the silicon nitride layer on a selected device. This will leave the device buried and able to function as a reference without the need for post-processing.

References

- [1] Y. Cui, Q. Q. Wei, H. K. Park, and C. M. Lieber, "Nanowire nanosensors for highly sensitive and selective detection of biological and chemical species," *Science*, vol. 293, no. 5533, pp. 1289–1292, 2001.
- [2] F. Patolsky, G. Zheng, and C. M. Lieber, "Nanowire sensors for medicine and the life sciences," *Nanomedicine*, vol. 1, no. 1, pp. 51–65, 2006.
- [3] Z. Li, Y. Chen, X. Li, T. I. Kamins, K. Nauka, and R. S. Williams, "Sequence-Specific Label-Free DNA Sensors Based on Silicon Nanowires," *Nano Letters*, vol. 4, no. 2, pp. 245–247, 2004.
- [4] E. Stern, J. F. Klemic, D. A. Routenberg, P. N. Wyrembak, D. B. Turner-Evans, A. D. Hamilton, D. A. LaVan, T. M. Fahmy, and M. A. Reed, "Label-free immunodetection with CMOS-compatible semiconducting nanowires," *Nature*, vol. 445, no. 7127, pp. 519–522, 2007.
- [5] J. F. Klemic, E. Stern, and M. A. Reed, "Hotwiring biosensors.," *Nature biotechnology*, vol. 19, no. 10, pp. 924–925, 2001.
- [6] E. T. Carlen and A. van den Berg, "Nanowire electrochemical sensors: can we live without labels?," *Lab on a Chip*, vol. 7, no. 1, pp. 19–23, 2007.
- [7] S. Chen, J. G. Bomer, E. T. Carlen, and A. Van Den Berg, "Al₂O₃/Silicon NanoISFET with Near Ideal Nernstian Response," *Nano Letters*, vol. 11, no. 6, pp. 2334–2341, 2011.
- [8] X. Bi, A. Agarwal, and K.-L. Yang, "Oligopeptide-modified silicon nanowire arrays as multichannel metal ion sensors," *Biosensors and Bioelectronics*, vol. 24, no. 11, pp. 3248–3251, 2009.
- [9] L. Luo, J. Jie, W. Zhang, Z. He, J. Wang, G. Yuan, L. C. M. Wu, and S.-T. Lee, "Silicon nanowire sensors for Hg²⁺ and Cd²⁺ ions," *Applied Physics Letters*, vol. 94, no. 19, 2009.
- [10] D. R. Kim, C. H. Lee, and X. L. Zheng, "Probing Flow Velocity with Silicon Nanowire Sensors," *Nano Letters*, vol. 9, no. 5, pp. 1984–1988, 2009.
- [11] Y. Paska, T. Stelzner, S. Christiansen, and H. Haick, "Enhanced Sensing of Nonpolar Volatile Organic Compounds by Silicon Nanowire Field Effect Transistors," *ACS Nano*, vol. 5, no. 7, pp. 5620–5626, 2011.
- [12] Y. Paska and H. Haick, "Interactive Effect of Hysteresis and Surface Chemistry on Gated Silicon Nanowire Gas Sensors," *ACS Applied Materials & Interfaces*, vol. 4, no. 5, pp. 2604–2617, 2012.
- [13] P. Bergveld, "Thirty years of ISFETOLOGY - What happened in the past 30 years and what may happen in the next 30 years," *Sensors and Actuators B-Chemical*, vol. 88, no. 1, pp. 1–20, 2003.
- [14] M. W. Shinwari, M. J. Deen, and D. Landheer, "Study of the electrolyte-insulator-semiconductor field-effect transistor (EISFET) with applications in biosensor design," *Microelectronics Reliability*, vol. 47, no. 12, pp. 2025–2057, 2007.

- [15] R. P. Feynman, R. B. Leighton, and M. Sands, *The Feynman Lectures on Physics*. 1977, pp. 10–1,9.
- [16] M. Mescher, L. C. P. M. de Smet, E. J. R. Sudhölter, and J. H. Klootwijk, “Robust fabrication method for silicon nanowire field effect transistors for sensing applications,” *To be published*, 2013.
- [17] M. Mescher, E. P. A. M. Bakkers, and J. H. Klootwijk, “Nanowire FETs as Sensor in a Liquid Environment,” Philips Research Europe Technical Note PR-TN 2009/00217.
- [18] M. Mescher, B. Marcelis, L. de Smet, E. J. R. Sudholter, and J. H. Klootwijk, “Pulsed Method for Characterizing Aqueous Media Using Nanowire Field Effect Transistors,” *IEEE Transactions on Electron Devices*, vol. 58, no. 7, pp. 1886–1891, 2011.
- [19] D. Beaumont, “Microfluidic disposable chip: concept design,” *Philips Research Process technology materials group*, 2011.
- [20] G. Åkerlöf and O. A. Short, “The Dielectric Constant of Dioxane—Water Mixtures between 0 and 80°,” *Journal of the American Chemical Society*, vol. 58, no. 7, pp. 1241–1243, Jul. 1936.
- [21] S. H. Pine, J. B. Hendrickson, D. J. Cram, and G. S. Hammond, *Organic Chemistry*, 4th ed. McGraw-Hill, 1980, p. 203.
- [22] “Shin-Etsu SIFEL.” [Online]. Available: <http://www.sifel.jp/products/sifel.shtml>.
- [23] R. S. Muller and T. I. Kamins, *Device Electronics for Integrated Circuits*, 2nd ed. .